

T-1141

DYNAMIC DEFORMATION OF COPPER

By

Conrad F. Fiftal

BOUND BY DENVER BOOKBINDING CO., 2727 - 17TH ST., DENVER, COLO. 80202

ProQuest Number: 10781600

All rights reserved

INFORMATION TO ALL USERS

The quality of this reproduction is dependent upon the quality of the copy submitted.

In the unlikely event that the author did not send a complete manuscript and there are missing pages, these will be noted. Also, if material had to be removed, a note will indicate the deletion.



ProQuest 10781600

Published by ProQuest LLC (2018). Copyright of the Dissertation is held by the Author.

All rights reserved.

This work is protected against unauthorized copying under Title 17, United States Code
Microform Edition © ProQuest LLC.

ProQuest LLC.
789 East Eisenhower Parkway
P.O. Box 1346
Ann Arbor, MI 48106 – 1346

A Thesis submitted to the Faculty and the Board of Trustees of the Colorado School of Mines in partial fulfillment of the requirements for the degree of Master of Science in Metallurgical Engineering.

Signed: Conrad F. Fiftal
Conrad F. Fiftal

Golden, Colorado

Date: Sept. 5, 1967

Approved: R. S. Culver
R. S. Culver
Thesis Advisor

A. W. Schlechten
A. W. Schlechten
Head of Department

Golden, Colorado

Date: Sept 5, 1967

ABSTRACT

An experimental technique has been developed for determining the dynamic flow stress of a metal, based upon the application of an energy balance to a bar-bar impact apparatus. The test specimen is compressed between two anvil bars by collinear impact. The geometry of the test system is controlled to give a plastic strain between 3 and 15%. A precise analysis of the kinetic and vibrational energy of the anvil bars before and after impact permits calculation of the work done in plastically deforming the specimen. Measurement of the final strain allows evaluation of the flow stress.

The rate sensitivity for cold-worked copper, defined as the slope of the log stress - log plastic strain rate curve at constant plastic strain, is shown to increase nonlinearly with both strain rate and temperature. At a temperature of 475°F the cold-worked copper recrystallizes during heating so that strain hardening occurs during subsequent deformation.

This strain hardening is taken into account in the calculation of rate sensitivity. At 75°F the rate sensitivity increases from a value of 0.02 in the strain rate range 10-100 sec⁻¹ to a value of 0.55 in the strain rate range 2000 - 5000 sec⁻¹. In the strain rate range 200 - 1200 sec⁻¹ the rate sensitivity for cold-worked copper is 0.10 at 75°F corresponding to a 26% increase in stress for a factor of 10 increase in rate, while at 475°F the rate sensitivity for recrystallized copper is 0.24 corresponding to a 73% increase in stress for a factor of 10 increase in rate. For a combination of high strain rate and high temperature it is expected that the rate sensitivity will approach a limiting value of unity corresponding to viscous flow.

Also included is a theoretical analysis of the collinear impact of two elastic bars separated by a yielding link.

TABLE OF CONTENTS

	Page
LIST OF FIGURES.	vii
LIST OF TABLES	ix
ACKNOWLEDGMENTS.	x
INTRODUCTION	1
MECHANICS OF BAR-BAR IMPACT.	6
General Equation of Wave Motion	6
Longitudinal Elastic Impact	8
Plastically Yielding Link	11
EXPERIMENTAL DETERMINATION OF FLOW STRESS AND STRAIN RATE	21
Flow Stress Determination	21
Energy Balance.	23
Kinetic Energy Evaluation.	23
Vibration Energy Evaluation.	25
Longitudinal vibration loss	26
Lateral vibration loss.	27
Plastic Work Evaluation.	30
Plastic Strain Determination.	31

	Page
Plastic Strain Rate Determination	32
EXPERIMENTAL APPARATUS	34
Specimen Design and Nominal Material Data	34
Impact Equipment.	37
Heating Equipment	39
Velocity Measuring Equipment.	42
Vibration Measuring Equipment	44
Lateral Strain Measuring Circuit	44
Longitudinal Strain Measuring Circuit.	45
Oscilloscope Sweep Triggering Circuit.	50
Plastic Strain Measuring Equipment.	52
EXPERIMENTAL PROCEDURE	53
EXPERIMENTAL RESULTS AND DISCUSSION.	55
Tests at 75°F	55
Tests at 475°F.	58
CONCLUSIONS.	62
APPENDICES:	
I. Tabulated Room Temperature Results of Previous Investigators.	64
II. Elastic Calibration Data.	70
III. 75°F Experimental Data.	72
IV. 475°F Experimental Data	75
V. Separation of Rate Sensitivity From Strain Hardening at 475°F	78
LITERATURE CITED	84

LIST OF FIGURES

Figure	Page
1. Velocities of Impacting Ends of Impact Bar and Specimen Bar, and Stress and Strain Rate in Specimen During First and Second Round-Trip Traverses of Stress Waves in the Elastic Bars	18
2. Static Stress-Strain Curves for Cold-Worked Copper	24
3. Bar-Bar Impact Apparatus	35
4. Nominal Recrystallization Data for Cold-Worked Copper.	36
5. Nominal Specimen Dimensions.	38
6. Air Gun Operation and Firing Sequence.	40
7. Impact Bar Muzzle Velocity Versus Air Gun Breech Pressure.	41
8. Drum Camera Trace.	43
9. Traces of Typical Strain Gauge Signals	46
10. Wheatstone Bridge Circuit for Measuring Longitudinal Vibrations.	48
11. Oscilloscope Sweep Triggering Circuit.	51
12. Stress Increase Ratio Versus Strain Rate for Copper at Room Temperature	57

Figure	Page
13. True Stress Versus Strain Rate for Copper at 475°F.	60
14. High Temperature Static Stress-Strain Curves for Cold-Worked Copper Exhibiting Strain Hardening	79
15. Determination of Strain Hardening Exponent and Stress Constant for Dynamic Tests at 475°F	83

LIST OF TABLES

Table	Page
1. Measured Elastic Calibration Data.	70
2. Calculated Elastic Calibration Data.	71
3. 75°F Measured Data	72
4. 75°F Calculated Data	73
5. Summary of 75°F Results.	56
6. 475°F Measured Data.	75
7. 475°F Calculated Data.	76
8. Summary of 475°F Results Neglecting Strain Hardening	59
9. Summary of 475°F Results Accounting for Strain Hardening	59

ACKNOWLEDGMENTS

The author wishes to express particular thanks to Dr. R. S. Culver, Professor of Basic Engineering, and to Dr. J. D. Lubahn, Professor of Metallurgical Engineering, for their continued interest and guidance during the course of this study.

Sincere appreciation is extended to Dr. M. W. Major, Professor of Geophysics, for his advice regarding preparation of the final manuscript.

The author wishes to gratefully acknowledge the Inland Steel Corporation whose financial assistance made this study possible.

Special thanks are extended to Dr. R. W. McAllister, Professor of Physics, for his suggestions regarding the design of the oscilloscope sweep triggering circuit; to Mr. H. E. Fletcher, Professor of Basic Engineering for his recommendations regarding induction heating; and to Mr. J. P. Kintner,

T-1141

Physics Machinist, for his technical assistance in the machining of specimens.

INTRODUCTION

Part of the energy which is received by the surface of a space vehicle from high intensity impact will be absorbed by the region adjacent to the surface in the form of plastic deformation and adiabatic heating and part will be transformed into kinetic and elastically stored energy in the form of a propagating stress wave. This stress wave has the potential of doing more serious damage (i.e. spalling) to the less rugged interior parts of the vehicle than the damage incurred by the more rugged exterior where the initial energy is absorbed. The plastic flow and adiabatic heating in the region near the surface will govern the intensity of the stress wave which propagates beyond the surface region. Thus the stress will only be as high as the plastic deformation resistance of the metal which in turn depends on two critical factors: strain rate and temperature. Rate sensitivity, defined as the slope of the log stress - log plastic strain rate curve at a particular strain, is known

to increase with both strain rate and temperature (Manjoine & Nadai, 1940). Therefore the rate sensitivity may be extremely high for a condition of both high strain rate and high temperature. Under those conditions a stress wave may have a very high intensity and high damage potential. Thus knowledge of the relationship between the variables of stress, strain, strain rate, and temperature in materials at large values of strain rate is necessary for design against spalling damage.

The present study was undertaken to determine the rate sensitivity of copper as a function of strain rate and temperature. A bar-bar impact apparatus was used to obtain dynamic strain rates which varied from 10^2 sec^{-1} to 10^3 sec^{-1} . A static strain rate of 10^{-4} sec^{-1} was obtained from a Baldwin-Emery SR-4 testing machine. Temperatures studied were 75°F and 475°F . Copper was chosen for this investigation because: (1) it is relatively free from impurities, (2) it has no energy absorbing phase transformation, (3) it is microstructurally stable at temperatures below the recrystallization temperature, and (4) it is a common test material.

The work of previous investigators at room temperature is tabulated in Appendix I. These results are compared with each other by the ratio of dynamic stress increase to static

stress ($S_p - S_o / S_o$) for a given strain and strain rate. At a strain rate of 100 sec^{-1} Straw (1965), using a split-Hopkinson bar apparatus found a stress increase of 26% while Bell & Werner (1962) using a similar system found no stress increase. One possible reason for this discrepancy is that Straw determined flow stress directly by means of an energy balance while Bell & Werner calculated stress indirectly from the double differentiation of a displacement-time curve. At a strain rate of 1000 sec^{-1} Ripperger (1965), Lindholm (1965), and Kolsky & Douch (1962) found stress increases of 40%, 23%, and 14% respectively. The tests of Ripperger and Lindholm differed only with respect to strain level; Ripperger had a plastic strain of 0.62 while Lindholm had a strain of 0.06. The tests of Lindholm and Kolsky & Douch differed with respect to test geometry. Lindholm used a loading pulse that was considerably longer than the length of the specimen thereby establishing uniform plastic strain throughout most of the deformation. Kolsky & Douch had a condition of nonuniform axial strain. At a strain rate of 2000 sec^{-1} Ripperger (1962) determined a stress increase of 60%. Although Kolsky (1949) had a plastic strain lower than Ripperger by a factor of 20 he found the stress to increase 113%. The main reason for this discrepancy is specimen geometry. Ripperger and Kolsky had length-to-diameter ratios

of 2.00 and 0.02 respectively. Kolsky's thin wafer exhibited transverse frictional effects, normally present at specimen-bar interfaces, throughout its length. Thus Kolsky had triaxial compression in contrast to the uniaxial stress of Ripperger.

It is obvious from the foregoing that correlation of results between investigators is difficult due to four factors: (1) flow stresses are determined by radically different methods, (2) different test geometries influence strain profiles, (3) different specimen geometries influence the state of stress, and (4) different plastic strain levels influence rate sensitivity.

In the present study a bar-bar impact apparatus was designed using a more fundamental and more direct approach than that used by most of the previous investigators. Also, results will be compared only with those investigators having similar testing conditions:

- (1) The test specimen will be compressed between two elastic anvil bars by collinear impact.
- (2) Flow stress will be determined directly from an energy balance of the entire test system.
- (3) The elastic anvil bars will be long compared to the specimen length so that strain will be uniform during deformation.

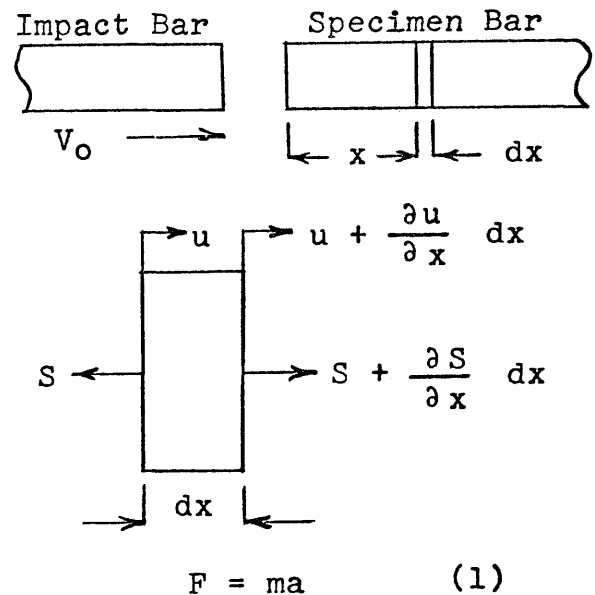
- (4) The length-to-diameter ratio for the specimen will be such that the stress state is uniaxial compression.
- (5) Results will be compared with other investigators at similar strain levels.

MECHANICS OF BAR-BAR IMPACT

This section will discuss the mechanics of bar-bar impact which is important to an understanding of how flow stress and strain rate will be experimentally determined in this investigation.

General Equation of Wave Motion

Consider an element of volume of the elastic specimen bar extending from (x) to $(x + dx)$. Stress, strain, velocity, displacement, and acceleration are all functions of both position (x) and time (t) . Newton's second law $F = ma$ can be applied to this element if we consider force and acceleration being positive to the right.



The net force to the right is

$$F = (S + \frac{\partial S}{\partial x} dx) A - SA = A \frac{\partial S}{\partial x} dx \quad (2)$$

where A is the cross-sectional area of the bar.

If u is the displacement to the right at any point x, the acceleration to the right is

$$a = \frac{\partial^2 u}{\partial t^2} \quad (3)$$

The mass is

$$m = (Adx) \rho \quad (4)$$

where ρ is mass density.

Substituting the values from Eq. (2), (3), and (4) into Eq. (1), we obtain

$$\frac{\partial S}{\partial x} = \rho \frac{\partial^2 u}{\partial t^2} \quad (5)$$

Stress and displacement can be related by using Hooke's law

$$S = Ee \quad (6)$$

where E is the elastic modulus and where strain, e, is related to displacement, u, by

$$e = \frac{L-L_0}{L_0} = \frac{[(x + dx + u + \frac{\partial u}{\partial x} dx) - (x + u)] - dx}{dx} = \frac{\partial u}{\partial x} \quad (7)$$

for any given time, t . By substituting Eq. (7) into Eq. (6), and Eq. (6) into Eq. (5), we obtain the "equation of motion" which expresses the single variable, u , as a function of x and t :

$$\frac{E}{\rho} \frac{\partial^2 u}{\partial x^2} = \frac{\partial^2 u}{\partial t^2} \quad (8)$$

Longitudinal Elastic Impact

Before applying this equation to the case of a "yielding link" (the test specimen) between the two elastic bars, the simpler case of elastic impact between the two bars will be considered, where the velocity of the impact bar is V_0 and the specimen bar is stationary. For this case the boundary conditions are

$$u = 0 \text{ for } t = 0 \text{ \& for all values of } x \quad (9)$$

$$\frac{\partial u}{\partial t} = 0 \text{ for } t = 0 \text{ \& for all plus } x\text{-values} \quad (10)$$

$$\frac{\partial u}{\partial t} = V_0 \text{ for } t = 0 \text{ \& for all minus } x\text{-values} \quad (11)$$

where positive x -values refer to locations in the specimen bar and negative x -values refer to locations in the impact bar. Also, at $x = 0$ there will be continuous contact; and this can be expressed by

$$\left(\frac{\partial u}{\partial t}\right)_{x = +dx} = \left(\frac{\partial u}{\partial t}\right)_{x = -dx} \quad (t > 0) \quad . \quad (12)$$

The solution for Eq. (8) using the boundary conditions in Eq. (9) - Eq. (12) indicates that u is a linear function of both x and t so that $\partial u / \partial x$ is a constant and the stress (S) generated in the bars is

$$\begin{aligned} S &= -k & (-b < x < b) \\ S &= 0 & \text{elsewhere} \end{aligned} \quad (13)$$

where b is a distance along the bars which is some function of t , and k is a constant; b and k now have to be determined. Since k is a constant for values of x from $x = -b$ to $x = b$, from Eq. (5) we find that the velocity of the material in the region $-b < x < b$ is constant and that it is moving as a rigid mass with the velocity of the interface between the two bars, V_I . Momentum balance requires that the momentum gain in the specimen bar equals momentum loss in the impact bar so that

$$\rho A b V_I = \rho A b (V_0 - V_I) \quad \text{or} \quad V_I = \frac{V_0}{2} \quad . \quad (14)$$

The interface moves to the right by an amount

$$u_I = \frac{kb}{E} \quad (15)$$

because of the elastic contraction of the material from $x = 0$ to $x = b$, and the corresponding work done on the specimen bar is .

$$(kA) \left(\frac{kb}{E} \right) = \frac{Ak^2b}{E} \quad (16)$$

This work equals the sum of the kinetic energy and elastically stored energy of the same region ($0 < x < b$)

$$\frac{Ak^2b}{E} = \frac{Ab\rho}{2} \left(\frac{V_0}{2} \right)^2 + \frac{Abk^2}{2E} \quad (17)$$

from which

$$k = \frac{V_0}{2} \sqrt{E\rho} \quad (18)$$

The distance b is governed by the fact that a length, $2b$, is shortening elastically, the point at $x = b$ is stationary, and the point $x = -b$ is continuously moving at a velocity, V_0 .

$$V_0 t = \frac{2bk}{E} = \left(\frac{2b}{E} \right) \left(\frac{V_0}{2} \right) \sqrt{E\rho} = V_0 b \sqrt{\frac{\rho}{E}} \quad (19)$$

from which

$$b = t \sqrt{\frac{E}{\rho}} = c_0 t \quad (20)$$

where c_0 is the acoustic wave velocity in the bar material.

Now, by substitution of Eq. (20) and Eq. (18) into the general solution of the wave equation, as expressed by Eq.

(13), we obtain

$$S = -\frac{V_0}{2} \rho c_0 (-c_0 t < x < c_0 t) \quad (21)$$

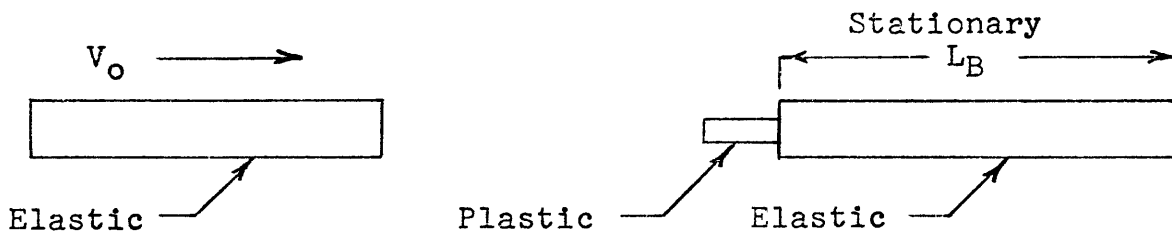
$S = 0$ and $V = 0$ or V_0 elsewhere.

These conditions will prevail until the boundary

between the stressed and unstressed material reaches the far end of each bar, that is, until $c_0 t = L_B$. At that point, it can be shown by similar methods that the interface between the stressed and unstressed material (the "wave front") moves back again toward the impacted end with the same velocity, c_0 , until both bars are unloaded (if they are equal in length) and their velocities have been interchanged.

Plastically Yielding Link

Consider the case where there is a yielding link (the test specimen) between two elastic bars of equal length.



If the specimen is short compared to the length of the elastic bars and if its rate of strain hardening is small, the strain and stress in the specimen will be uniform with length and independent of time. In this case, each elastic bar will experience the same constant force as the specimen deforms plastically if the area change is negligible. This force is the flow stress (S_p) in the specimen times the area (A_p) of the specimen.

For the two elastic bars, the same differential equation, Eq. (8), with the same solution Eq. (13), applies; but now the boundary conditions are different. For each bar, the uniformly compressed region is moving as a rigid body if considered at any specified value of time. Let these velocities be V_i for the impact bar and V_s for the specimen bar. The specimen bar will be considered first.

The velocity, V_s , of the compressed portion of the specimen bar can be determined by applying an energy balance to the specimen bar. The work done at the impacted end is

$$\text{force} \times \text{distance} = (S_p A_p) (V_s t)$$

and this work equals the sum of the kinetic energy and elastically stored energy. If k is the compressive stress in the compressed region and b is the length of the compressed region, these energies are

$$\text{kinetic energy} = \frac{1}{2} (Ab\rho) V_s^2$$

$$\text{elastically stored energy} = (Ab) \left(\frac{k^2}{2E} \right) .$$

The energy balance can then be expressed as

$$(S_p A_p)(V_s t) = \frac{1}{2} (Ab\rho) V_s^2 + (Ab) \left(\frac{k^2}{2E} \right) . \quad (22)$$

The unknowns k and b can be determined from force equilibrium and compatibility.

$$\text{force equilibrium: } S_p A_p = kA \quad (23)$$

The compatibility condition is expressed by the fact that the change in length of the compressed region equals the motion of the impacted end:

$$\left(\frac{k}{E}\right) (b) = V_s t \quad (24)$$

Solving Eq. (23) and Eq. (24) for k and b , we obtain

$$k = \frac{S_p A_p}{A} \quad \text{and} \quad b = \frac{E V_s t A}{S_p A_p} .$$

Substituting into Eq. (22) and solving for V_s ,

$$V_s = \frac{S_p A_p}{A} \sqrt{\frac{1}{E \rho}} . \quad (25)$$

Note from Eq. (24) that the location, b of the wave front is proportional to time, that is, that the wave front velocity is a constant. Calling this wave front velocity c_o , we find its value to be

$$c_o = \frac{b}{t} = \frac{E V_s A}{S_p A_p} = \frac{EA}{S_p A_p} \left(\frac{S_p A_p}{A} \sqrt{\frac{1}{E \rho}} \right) = \sqrt{\frac{E}{\rho}}$$

which is the same as in elastic impact (see Eq. 20).

In terms of c_o , the expression for V_s becomes

$$V_s = \frac{S_p A_p}{A \rho c_o} . \quad (26)$$

In a similar manner, for the impact bar

$$V_1 = V_o - \frac{S_p A_p}{A \rho c_o} . \quad (27)$$

Therefore, the change in velocity of both bars, ΔV , is the same

$$\Delta V = \frac{S_p A_p}{A_p c_o} \quad (28)$$

Summarizing:

	impact bar	specimen bar
compressive stress	$\frac{S_p A_p}{A}$	$\frac{S_p A_p}{A}$
compressed length	$c_o t$	$c_o t$
impacted end velocity	$V_o - \Delta V$	ΔV

The strain rate in the specimen is

$$\dot{\epsilon} = \frac{d\epsilon}{dt} = \frac{1}{dt} \left(\frac{dL_p}{L_p} \right) = \frac{1}{L_p} \left(\frac{dL_p}{dt} \right) = \frac{1}{L_p} (V_i - V_s) \quad (29)$$

where ϵ is logarithmic plastic strain and L_p is the instantaneous length of the specimen. Substituting the velocities from Eq. (26) and Eq. (27) into Eq. (29)

$$\dot{\epsilon} = \frac{1}{L_p} (V_o - 2 \Delta V) \quad (30)$$

This strain rate will prevail until the reflected waves from the free ends of the elastic bars reach the specimen, that is, at $t = 2L_B/c_o$ after impact. The strain during this time can be controlled independently of the strain rate by varying the length of the elastic bars. The conditions

governing the action of the system at this point will depend upon the relative magnitudes of V_0 and ΔV . By methods similar to those used previously, it can be shown that velocity of the specimen bar behind the reflected wave front is $2 \Delta V$, while for the projectile it is $V_0 - 2 \Delta V$. Thus, when the reflected waves reach the specimen, both elastic bars will be completely unloaded and will have a relative velocity of

$$V_{rel} = V_0 - 4 \Delta V \quad . \quad (31)$$

Note that ΔV , according to Eq. (27), depends only on the dimensions and properties of the specimen and the elastic bars, and that both strain rate and final relative velocity (after unloading of the two elastic bars) depend only on specimen length, V_0 , and ΔV , as indicated by Eq. (30) and Eq. (31). This means that, once the specimen and the two elastic bars have been specified, the behavior of the system will depend only on the initial velocity, V_0 , of the impact bar. This behavior can be visualized in terms of progressively larger values of V_0 . For $V_0 < 2 \Delta V$, the stress in the specimen will be less than the yield strength, and plastic flow will not occur. The stress (S) in the specimen for $V_0 < 2 \Delta V$ can be found from Eq. (18) and Eq. (23):

$$S = k \left(\frac{A}{A_p} \right) = \left(\frac{A}{A_p} \right) \left(\frac{V_0}{2} \right) \sqrt{E\rho} \quad .$$

This stress is proportional to the initial velocity, V_0 , and becomes equal to the yield strength (S_p) of the specimen for the case where V_0 has twice the value given by Eq. (25). In this range $0 < V_0 < 2\Delta V$, the relative velocity after return of the reflected waves is the negative of the initial velocity, V_0 . For the case where V_0 is just twice the value given by Eq. (25), the final relative velocity of $(-2\Delta V)$ can also be obtained from Eq. (31), and the fact that there is no plastic flow is borne out by $\dot{\epsilon} = 0$ as obtained from Eq. (30). As V_0 increases above $2\Delta V$, plastic flow occurs in the specimen at a faster and faster rate, as given by Eq. (30), and the final relative velocity becomes smaller and smaller, as given by Eq. (31). For $V_0 = 4\Delta V$, the relative velocity after impact becomes zero, that is, the two elastic bars are moving together in an unstressed condition, each at one-half the velocity which the projectile had initially.

For a still larger V_0 ($V_0 > 4\Delta V$), the two elastic bars are still moving together after the first cycle ($t = 2L_B/c_0$), and so the specimen receives a second impact. The stress attained by the specimen during this second cycle increases, as V_0 increases above $4\Delta V$, until it reaches the yield strength when the relative velocity after the first cycle reaches $2\Delta V$ (i.e. when $V_0 = 6\Delta V$). Thus, plastic flow will occur in

the specimen once, and only once, for V_0 -values between $2\Delta V$ and $6\Delta V$, and the strain rate can have a certain corresponding range of values as given by Eq. (30). Fig. 1 shows the effect of increasing V_0 on relative velocity, specimen stress, and specimen strain rate, expressed in terms of ΔV as given by Eq. (28).

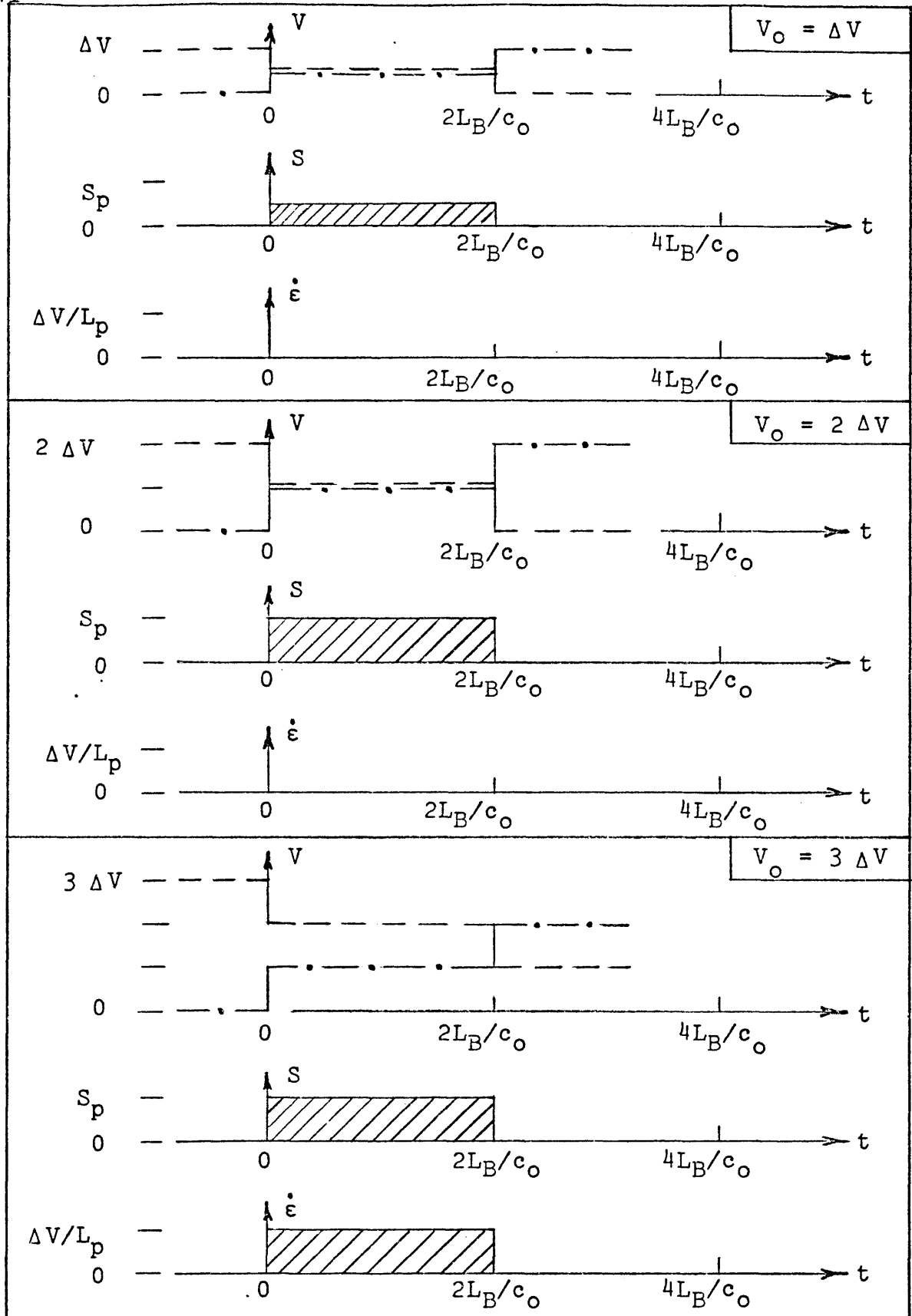


Figure 1. Velocities of Impacting Ends of Impact Bar (dashed) & Specimen Bar (dot-dash), and Stress & Strain Rate in Specimen During First and Second Round-Trip Traverses of Stress Waves in the Elastic Bars.

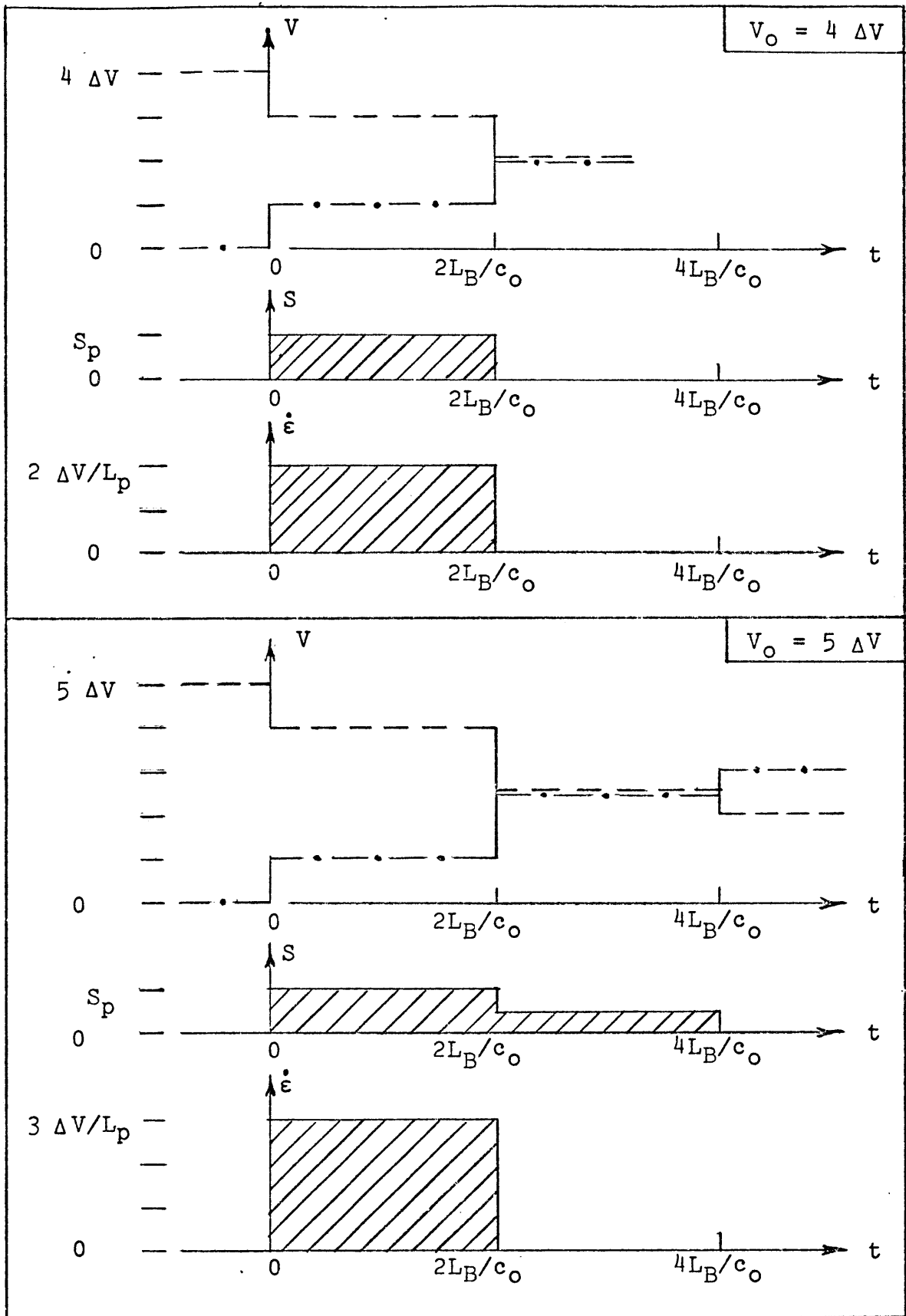


Figure 1. (continued)

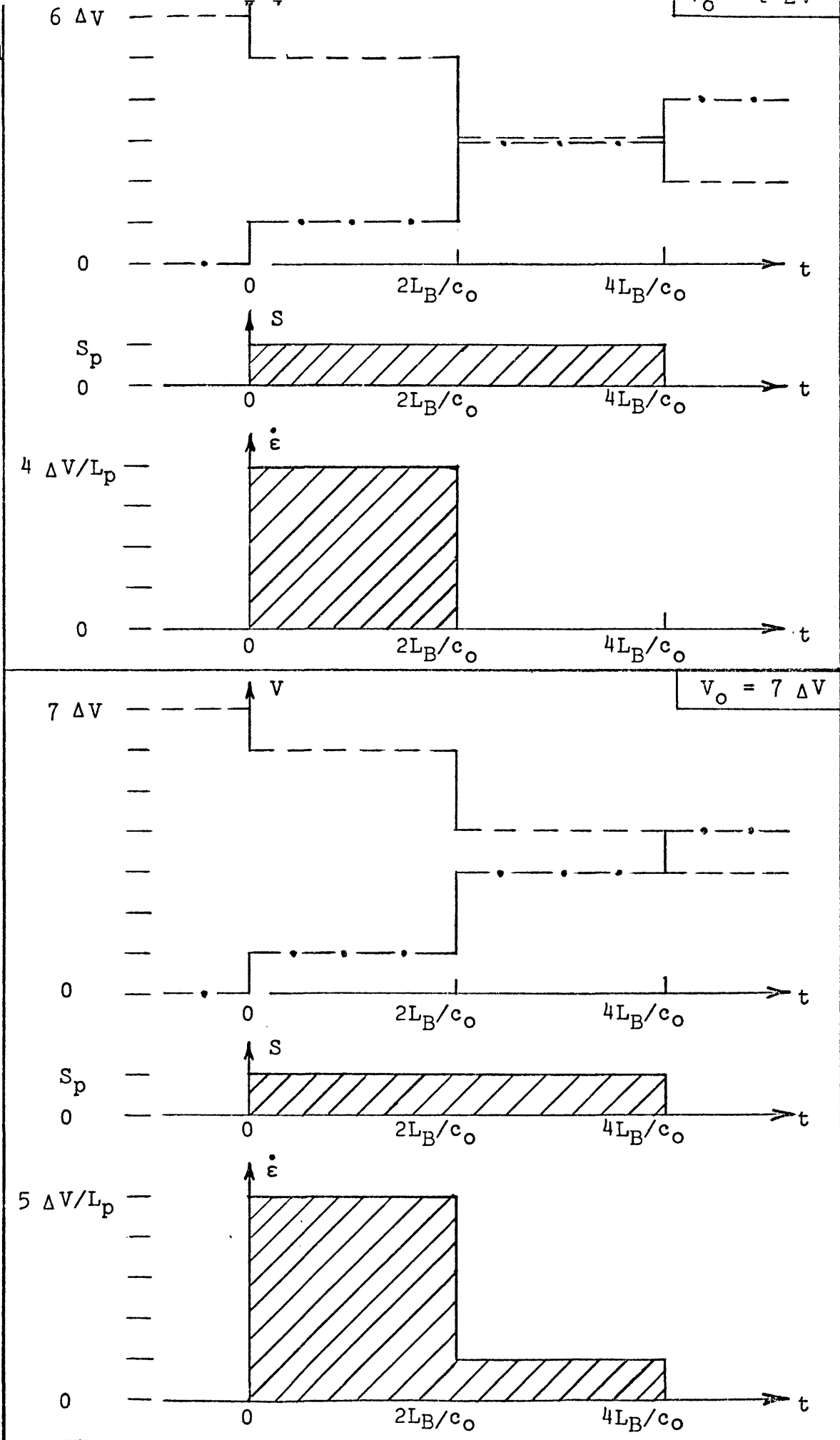


Figure 1. (continued)

EXPERIMENTAL DETERMINATION OF
FLOW STRESS AND STRAIN RATE

In the previous section the mechanics of a plastically yielding specimen compressed between two elastic bars by collinear impact were analyzed. An experimental method for determination of flow stress and strain rate for such a system will now be presented.

Flow Stress Determination

Flow stress can be determined from the energy associated with plastic deformation of the specimen. The plastic work is given by

$$E_p = \int_{L_0}^{L_f} F \, dL_p \quad (32)$$

where F is the force on the specimen, L_0 is the initial length of the specimen, and L_f is the final specimen length.

Expressing the force in terms of the true stress (S_p)

and instantaneous cross-sectional area (A_p) we have

$$F = S_p A_p \quad . \quad (33)$$

The infinitesimal plastic length change of the specimen (dL_p) may be related to the infinitesimal axial logarithmic plastic strain ($d\epsilon_a$) and to the instantaneous specimen length (L_p) by

$$dL_p = L_p d\epsilon_a \quad . \quad (34)$$

By substituting Eq. (33) and Eq. (34) into Eq. (32) and changing the limits of integration the plastic work may be expressed by

$$E_p = \int_0^{\epsilon_a} A_p L_p S_p d\epsilon_a \quad . \quad (35)$$

Since the specimen volume is constant for plastic deformation the product $A_p L_p$ is independent of strain and Eq. (35) may be written as

$$\frac{E_p}{\text{vol}} = \int_0^{\epsilon_a} S_p d\epsilon_a \quad . \quad (36)$$

Cold-worked copper was used in this investigation so that the static flow stress would be essentially independent of strain over a temperature range $75^\circ\text{F} < T < 400^\circ\text{F}$ as shown in

Fig. 2. It was assumed that the dynamic flow stress, although higher, is also independent of strain so that Eq. (36) can be rewritten in the form

$$S_p = \frac{E_p}{(\text{vol}) \epsilon_a} \quad 75^\circ\text{F} < T < 400^\circ\text{F} \quad . \quad (37)$$

Once the plastic deformation energy and plastic strain are determined the flow stress can be evaluated from Eq. (37).

Energy Balance

The plastic work (E_p) is determined by applying an energy balance to the bar-bar impact system. For an adiabatic process the first law of thermodynamics states that the work done by a system is equal to the change in energy for that system. This can be expressed as

$$E_p = KE_o - KE_i - KE_s - E_v \quad (38)$$

where KE_o , KE_i , and KE_s are the kinetic energies of the impacting bar before impact, the impacting bar after impact, and the specimen bar after impact respectively and where E_v is the vibrational energy loss after impact. The plastic work (E_p) can be evaluated from Eq. (38) once the other terms are known.

Kinetic Energy Evaluation

The kinetic energies of the bars can be determined by measuring their respective velocities before and after impact.

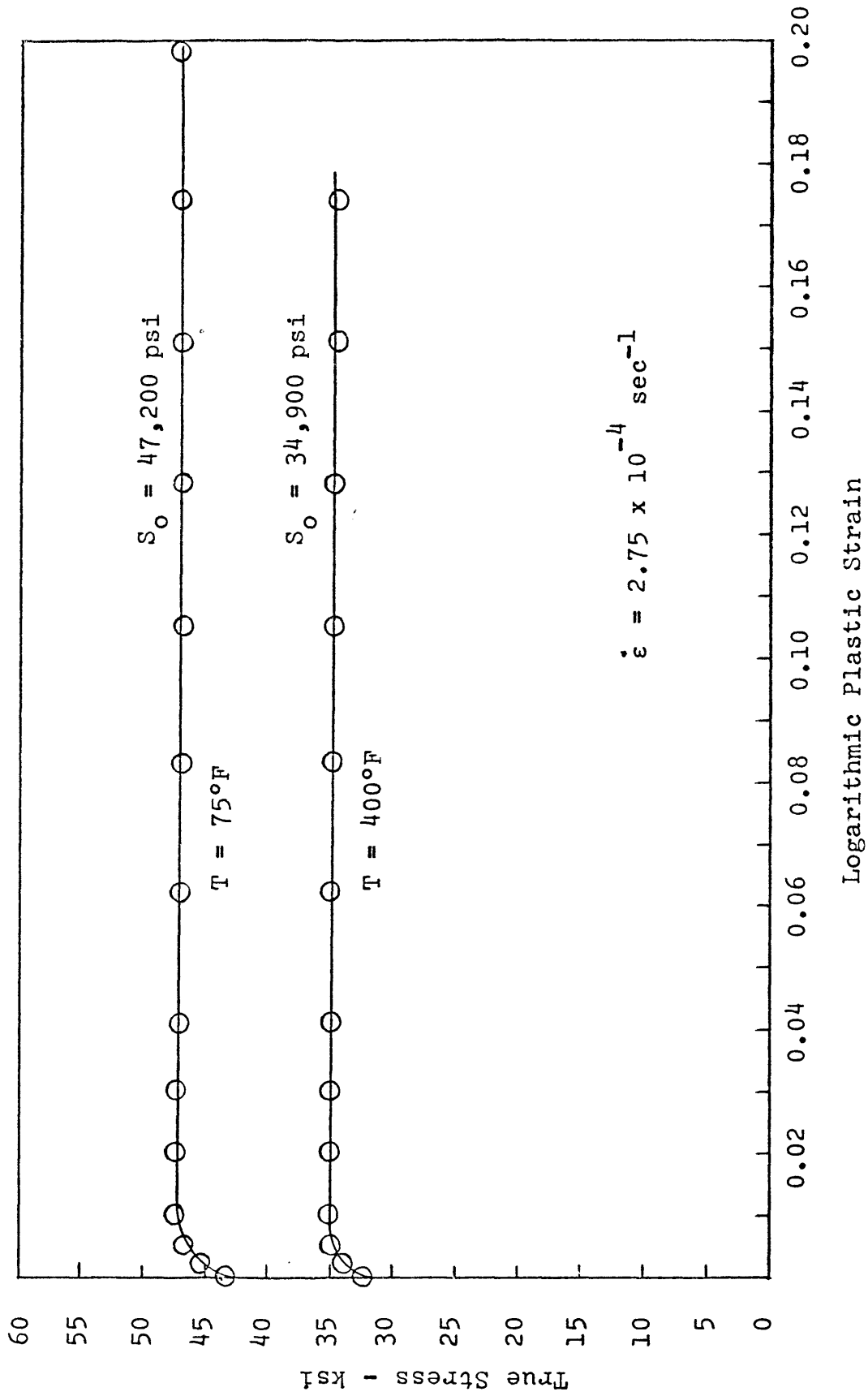


Figure 2. Static Stress-Strain Curves for Cold-worked Copper.

These measurements were made with a drum camera which photographed the displacement of the ends of the bars within a calibrated time scale. The following equations will apply:

$$KE_0 = \frac{1}{2} M_i V_0^2 \quad (39)$$

$$KE_1 = \frac{1}{2} M_i V_1^2 \quad (40)$$

$$KE_s = \frac{1}{2} M_s V_s^2 \quad (41)$$

where V_0 , V_1 , and V_s are the velocities of the impact bar before impact, the impact bar after impact and the specimen bar after impact respectively and where M_i and M_s are the masses of the impact bar and specimen bar respectively.

Vibration Energy Evaluation

For an ideal collinear impact there should be no residual elastic strain present in the bars when they separate that may give rise to vibrations. However, due to imperfections in the experiment, 2% of the initial kinetic energy was lost as vibrational energy. The vibrations were of two distinct and independent types: longitudinal and lateral. The longitudinal vibrations were primarily the result of differences in geometry between the bars (i.e. Aluminum spacers were attached around the impact bar in order to guide it down the barrel of the air gun). These vibrations were quite reproducible due to the fact that the longitudinal elastic stress generated in the bars was only a function of

the flow stress of the specimen. The lateral vibrations varied somewhat from test to test and were found to depend upon the bar alignment and the impact velocity. The total vibrational energy loss (E_v) was taken as the sum of the longitudinal and lateral components.

$$E_v = E_{\text{long}} + E_{\text{lat}} \quad (42)$$

where E_{long} is the longitudinal energy loss and E_{lat} is the lateral energy loss. Determination of vibration losses was based on oscilloscope strain-time records obtained from semiconductor strain gauges mounted on the specimen bar measuring longitudinal and lateral surface strains.

Longitudinal vibration loss

The longitudinal vibration loss (E_{long}) was assumed to be equal to the maximum elastically stored longitudinal strain energy in the bars when they separate. This is described by the equation

$$E_{\text{long}} = \frac{1}{2} E e_{\text{long}}^2 (\text{vol}) \quad (43)$$

where E is the elastic modulus for the bars, e_{long} is the longitudinal elastic strain, and vol is the volume of both bars.

The longitudinal elastic strain (e_{long}) is related to the longitudinal strain amplitude ($A_{m_{\text{long}}}$) as measured from oscilloscope records by

$$e_{\text{long}} = \frac{2 (VS)}{I_g R_g K_g} (Am_{\text{long}})^* \quad (44)$$

where VS is the vertical sensitivity of the oscilloscope (volts/cm), R_g is the strain gauge resistance (ohms), K_g is the strain gauge amplification factor, and I_g is the current through the gauge (amps).

Substituting Eq. (44) into Eq. (43) the longitudinal vibration loss is given by

$$E_{\text{long}} = \frac{2E (\text{vol}) (VS)^2}{I_g^2 R_g^2 K_g^2} (Am_{\text{long}})^2 \quad (45)$$

For the experimental conditions where E is 30×10^6 psi, vol is $3\pi/2$ in³, VS is 0.01 volts/cm, I_g is 0.0115 amps, R_g is 250 ohms, and K_g is 115.8 the longitudinal vibration loss can be evaluated from

$$E_{\text{long}} = 0.255 (Am_{\text{long}})^2 \quad (46)$$

Lateral vibration loss

The lateral vibration loss is equal to the maximum total bending strain energy in both bars when they separate. Since the lateral strain distribution along the length of

*The longitudinal strain measuring circuit and the derivation of this equation are described in detail in the section entitled "Experimental Apparatus".

the bars is unknown, the bending strain energy (E_b) can only be determined for a small finite length of bar in the cross-section of maximum lateral surface strain (e_s) that is given by

$$E_b = \frac{E(\text{vol})}{16} e_s^2$$

where vol is a small finite volume.

Assuming that the lateral strain distribution along the bars stays the same in all tests, the square of the maximum lateral surface strain is still proportional to the lateral vibration loss (E_{lat}) so that

$$E_{\text{lat}} = C e_s^2$$

where C is a proportionality constant.

The strain gauges may not necessarily be in the position of maximum lateral surface strain, but the measured lateral strain amplitude (Am_{lat}) is still a relative measure of the lateral vibration loss from test to test so that

$$E_{\text{lat}} = K(Am_{\text{lat}})^2 = K(Am_x^2 + Am_y^2)^* \quad (47)$$

where Am_x and Am_y are the horizontal and vertical components of the lateral strain amplitude respectively and K is a new proportionality constant to be determined.

*The lateral strain measuring circuit is described in detail in the section entitled "Experimental Apparatus".

The constant K is evaluated from an independent measure of the energy loss corresponding to a given lateral vibration signal. By replacing the yielding copper specimen with an identical hardened steel specimen, it was possible to obtain a perfectly elastic impact. For this situation there is no plastic work done and the impacting bar comes to rest during impact so that Eq. (38) reduces to

$$KE_0 - KE_s - E_v = 0. \quad (48)$$

By adjusting the impact velocity to the proper value it is possible to obtain the same longitudinal stress amplitude generated in the bars as they experienced during a plastic test. The vibration signals thus obtained are comparable to those obtained from a plastic test, the main difference being in the duration of impact.

The elastic calibration data is given in Tables 1 and 2, Appendix II. The total vibration energy loss was determined from Eq. (48). The lateral vibration loss was evaluated from Eq. (42) by subtracting the longitudinal vibration loss as given by Eq. (46) from the total vibration energy. The constant K was calculated to be 4.24 in-lb/cm^2 from Eq. (47) for an average lateral strain amplitude corresponding to an average lateral vibration loss. Thus Eq. (47) can be written as

$$E_{\text{lat}} = 4.24 (A_{\text{mlat}})^2 = 4.24 (A_{\text{x}}^2 + A_{\text{y}}^2), \quad (49)$$

and can be used to determine the lateral vibration loss for the plastic tests.

Plastic Work Evaluation

The equation necessary for the determination of the energy of plastic deformation will now be summarized as follows:

$$E_{\text{p}} = KE_{\text{O}} - KE_{\text{i}} - KE_{\text{s}} - E_{\text{v}} \quad (50)$$

$$KE_{\text{O}} = \frac{1}{2} M_{\text{i}} V_{\text{O}}^2 \quad (51)$$

$$KE_{\text{i}} = \frac{1}{2} M_{\text{i}} V_{\text{i}}^2 \quad (52)$$

$$KE_{\text{s}} = \frac{1}{2} M_{\text{s}} V_{\text{s}}^2 \quad (53)$$

$$E_{\text{v}} = E_{\text{long}} + E_{\text{lat}} \quad (54)$$

$$E_{\text{long}} = 0.255 (A_{\text{mlong}})^2 \quad (55)$$

$$E_{\text{lat}} = 4.24 (A_{\text{mlat}})^2 \quad (56)$$

A further simplification can be made: Since the longitudinal vibration energy comprises only 0.5% of the total vibration energy (Table 2, Appendix II), it can be neglected. Thus Eq. (55) can be deleted and Eq. (54) modified to read

$$E_{\text{v}} = E_{\text{lat}} \quad (57)$$

Plastic Strain Determination

The axial plastic strain was most reliably determined by first measuring the radial strain because:

1. Averaging many diameter measurements, each of which represents the total strain in the specimen gave a better average value than one length measurement.
2. An effective gauge length in the axial direction was difficult to determine due to the specimen end being machined with a slightly conical crown to minimize lateral vibrations.

The logarithmic radial plastic strain is given by

$$\epsilon_r = \ln \frac{D_{avg}}{D_0} \quad (58)$$

where D_0 is the initial diameter of the specimen and D_{avg} is the final average diameter determined by measuring the diameter at intervals along the specimen axis and averaging the readings. Diameter measurements were made on two perpendicular axes to account for any out-of-roundness of the deformed specimen.

From the constant volume condition for logarithmic plastic strains we have

$$\epsilon_a + \epsilon_r + \epsilon_t = 0$$

where ϵ_a is the axial strain, ϵ_r is the radial strain, and ϵ_t is the tangential strain. But for solid rods under

uniaxial stress

$$\epsilon_r = \epsilon_t \cdot$$

Therefore the axial logarithmic strain necessary for determination of the flow stress can be evaluated from

$$\epsilon_a = -2 \epsilon_r \cdot \quad (59)$$

Plastic Strain Rate Determination

Once the flow stress (S_p) has been determined from Eq. (37) the change in velocity of the two ends of the elastic bars (ΔV) in contact with the specimen during the time of plastic yielding can be evaluated from Eq. (28)

$$\Delta V = \frac{A_p S_p}{A \rho c_0} \quad (60)$$

where A_p/A is a ratio of the cross-sectional area of the specimen to the cross-sectional area of the elastic bars, ρ is the mass density of the bar material, and c_0 is the acoustic wave velocity in the bars. The onset of loading in the elastic bars is staggered by the time required for an elastic wave to travel the length of the specimen, but since this is only 3% of the total loading time it can be ignored.

The plastic strain rate ($\dot{\epsilon}$) can be expressed, from Eq. (30) in terms of the velocities of the two ends of the yielding specimen by

$$\dot{\epsilon} = \frac{V_0 - 2\Delta V}{L_p} \quad 2\Delta V < V_0 < 6 \Delta V \quad (61)$$

where V_0 is the impact velocity and L_p is the instantaneous specimen length which changes from an initial length L_0 to a final length $L_0 \ln^{-1} \epsilon_a$ during the impact. Rewriting Eq. (61) in terms of the average length we have

$$\dot{\epsilon}_1 = \frac{2 (V_0 - 2\Delta V)}{L_0 + L_0 \ln^{-1} \epsilon_a} \quad (62)$$

where ϵ_a is the axial logarithmic strain.

The average strain rate ($\dot{\epsilon}_1$) evaluated from Eq. (62) should compare closely with the strain rate ($\dot{\epsilon}_2$) determined by dividing the axial strain by the time of straining as given by

$$\dot{\epsilon}_2 = \frac{\epsilon_a c_0}{2 L_B} \quad (63)$$

where L_B is the length of the elastic bars.

EXPERIMENTAL APPARATUS

The bar-bar impact apparatus used in this investigation is shown in Fig. 3. The equipment and materials used will be discussed as follows:

- (1) Specimen Design and Nominal Material Data
- (2) Impact Equipment
- (3) Heating Equipment
- (4) Velocity Measuring Equipment
- (5) Vibration Measuring Equipment
- (6) Plastic Strain Measuring Equipment

Specimen Design and Nominal Material Data

Specimens were made from 1/2 in. diam tough-pitch copper bar stock that had been cold-drawn 45% corresponding to a plastic strain of 0.60. Figure 4 indicates that recrystallization begins in this material (for zero applied stress) at 500°F. Presumably testing may be carried out at temperatures up to 500°F without introducing the complications of

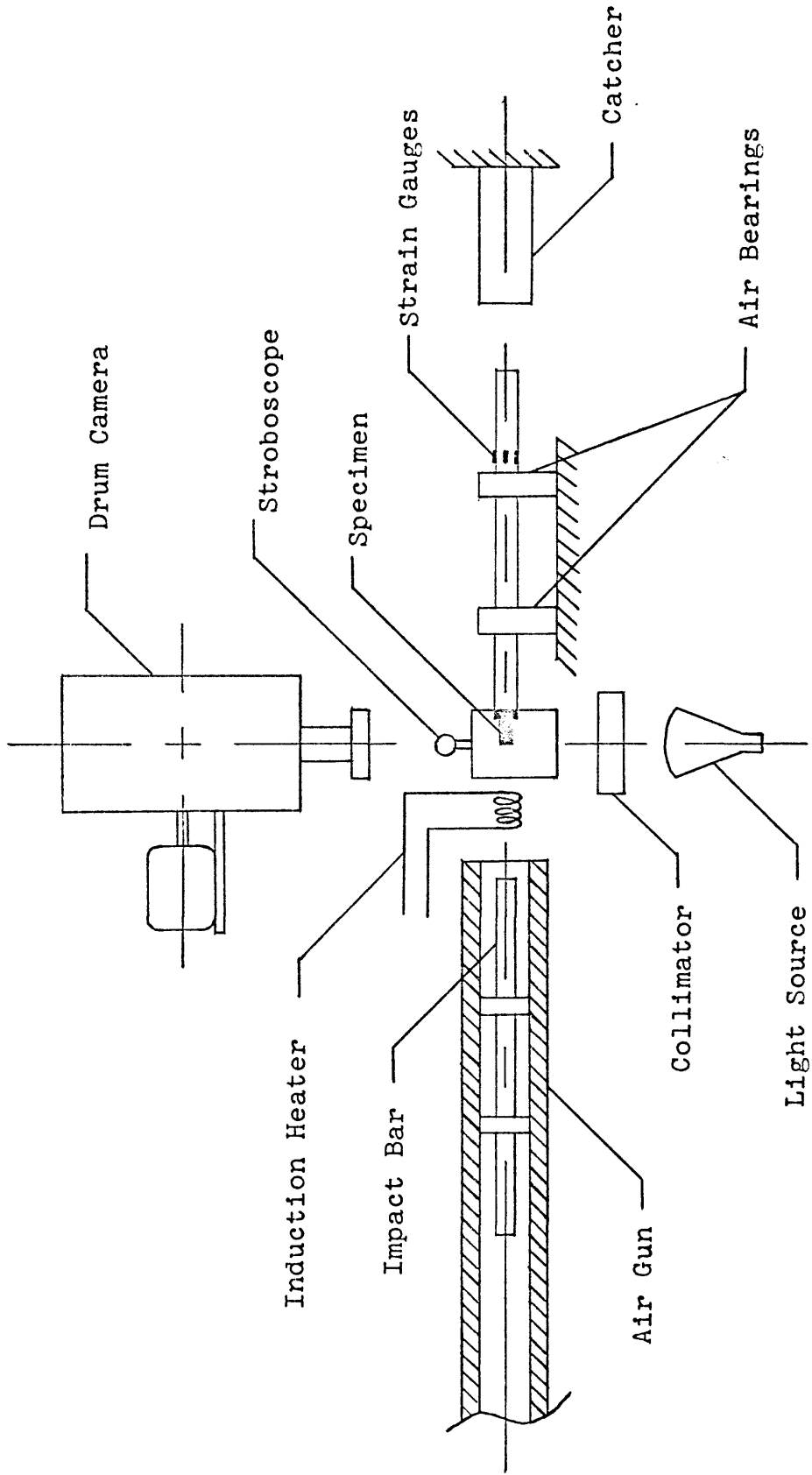


Figure 3. Bar-Bar Impact Apparatus.

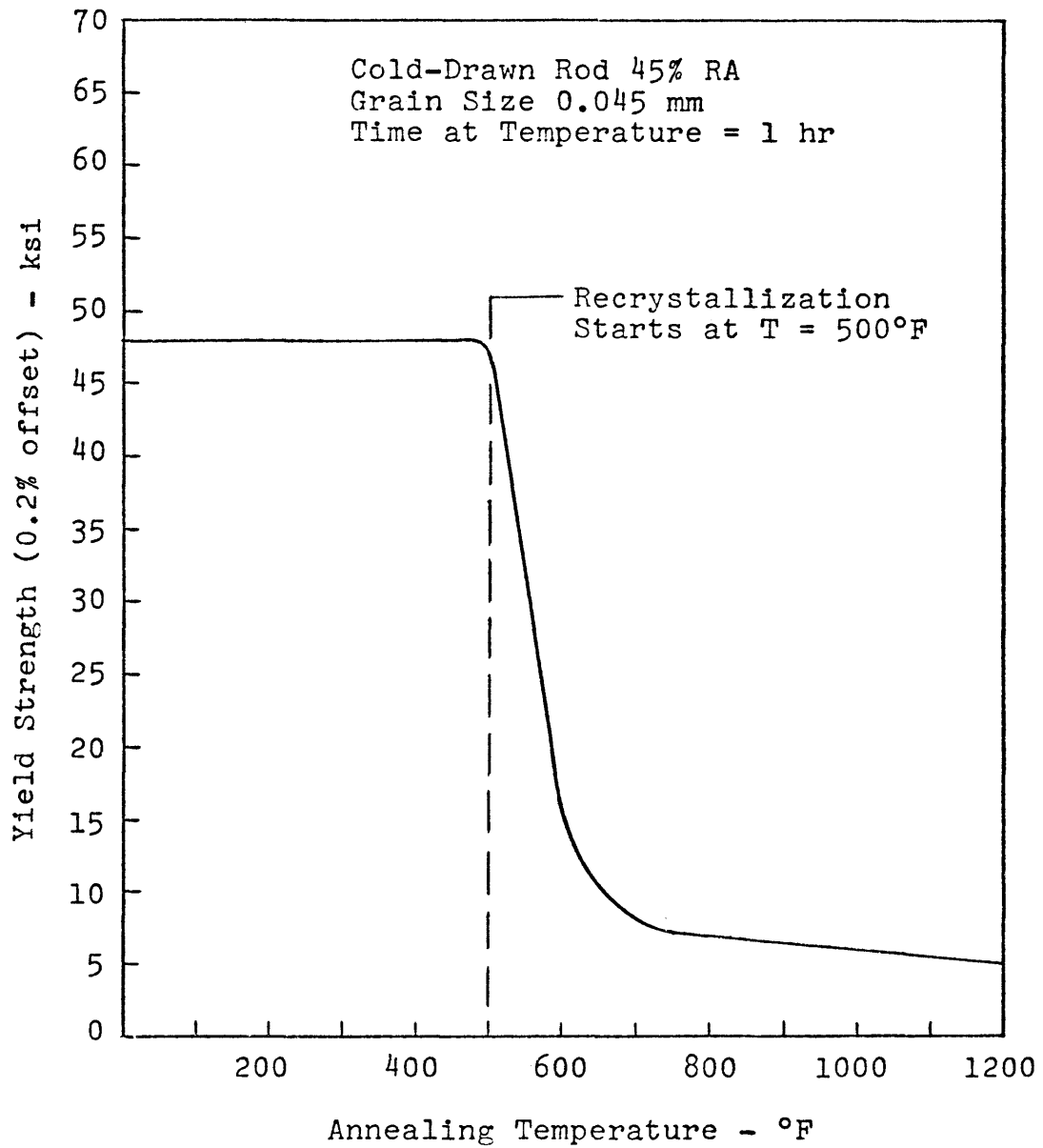


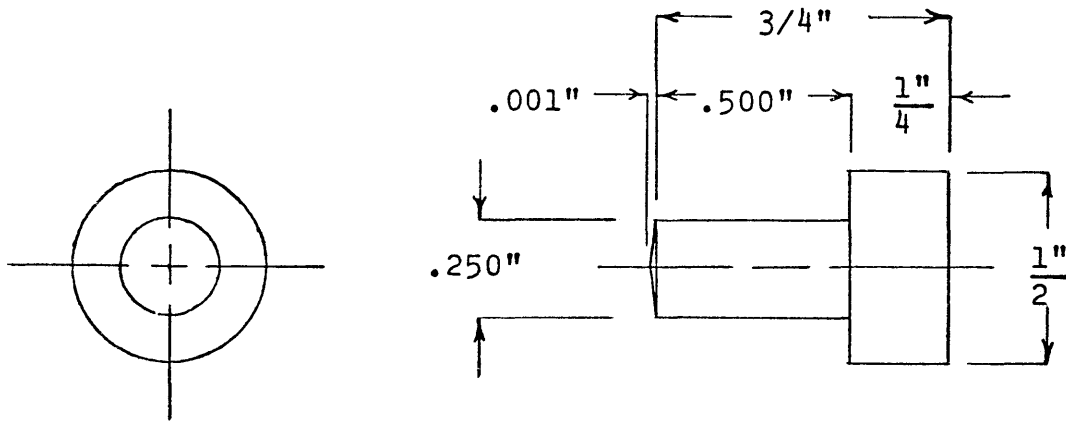
Figure 4. Nominal Recrystallization Data for Cold-Worked Copper (Wilkins & Bunn, 1943).

a metallurgical structure change.

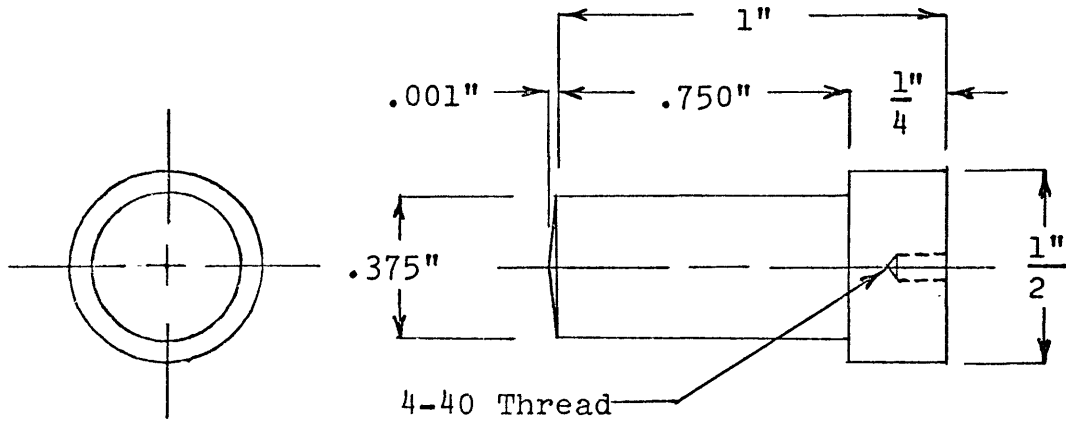
T-head specimens were machined to the nominal dimensions shown in Fig. 5. A length-to-diameter ratio of 2 was used as an acceptable compromise between the radial constraint found in a lower ratio and the buckling tendencies of a long specimen. The specimen length is short compared to the length of the elastic bars so that the strain will be essentially uniform during deformation. The end of the specimen was made slightly conical in shape to assure axially of impact. Since preliminary testing showed that the average high temperature dynamic flow stress was approximately four-ninths of the average room temperature dynamic flow stress the area ratio of the specimens was made $9/4$ so that the same longitudinal stress amplitude would be generated in the elastic bars during both tests. The room temperature specimens were glued onto the end of the specimen bar with Eastman 910 adhesive. The bases of the high temperature specimens were threaded so that they could be screwed onto the specimen bar since the adhesive loses its bonding characteristics above 200°F .

Impact Equipment

An air gun was used to fire a $1/2$ in. diam-12 in. long hardened steel impact bar at a copper specimen mounted on



Room Temperature Specimen T = 75°F



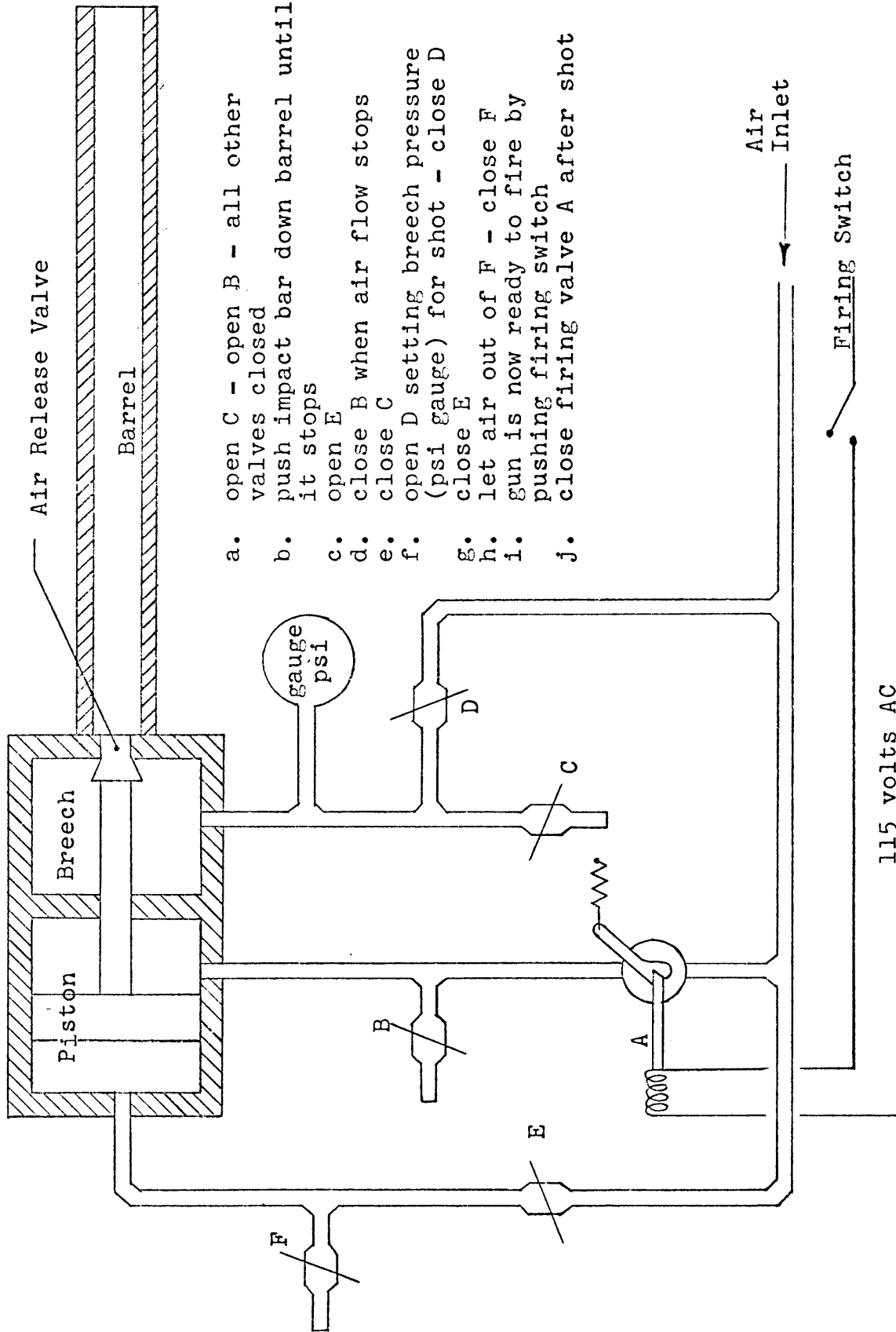
High Temperature Specimen T = 475°F

Figure 5. Nominal Specimen Dimensions.

the end of a similar steel specimen bar. The weight of each bar was 0.776 lbs. The impact bar was supported by two snug fitting aluminum spacers which centered the bar in the 1 1/2 in. diam bore of the air gun. The specimen bar was supported by two air bearings which were carefully aligned with the axis of the air gun. A catcher consisting of a pipe filled with modeling clay stopped the specimen bar after a free flight of 2 in. The operation of the air gun and firing sequence is illustrated in Fig. 6. Impact bar muzzle velocity was calibrated as a function of breech pressure (Fig. 7) so that particular impact velocities could be reproduced at any time. A momentum balance for each test was used to check the degree of isolation of the bar-bar impact from the surroundings.

Heating Equipment

The specimens were heated with a water-cooled induction coil of 1/8 in. diam copper tubing powered by an Ajax-Northrup high frequency induction converter. A potential of 2200 volts was discharged through an 8.0 μ h induction coil. The coil consisted of 26.5 turns having a 1 7/16 in. diam within a 3.8 in. length. The heating time to temperature was approximately 3 min. The surface temperature was measured with a thermocouple and potentiometer.



- a. open C - open B - all other valves closed
- b. push impact bar down barrel until it stops
- c. open E
- d. close B when air flow stops
- e. close C
- f. open D setting breech pressure (psi gauge) for shot - close D
- g. close E
- h. let air out of F - close F
- i. gun is now ready to fire by pushing firing switch
- j. close firing valve A after shot

Figure 6. Air Gun Operation and Firing Sequence.

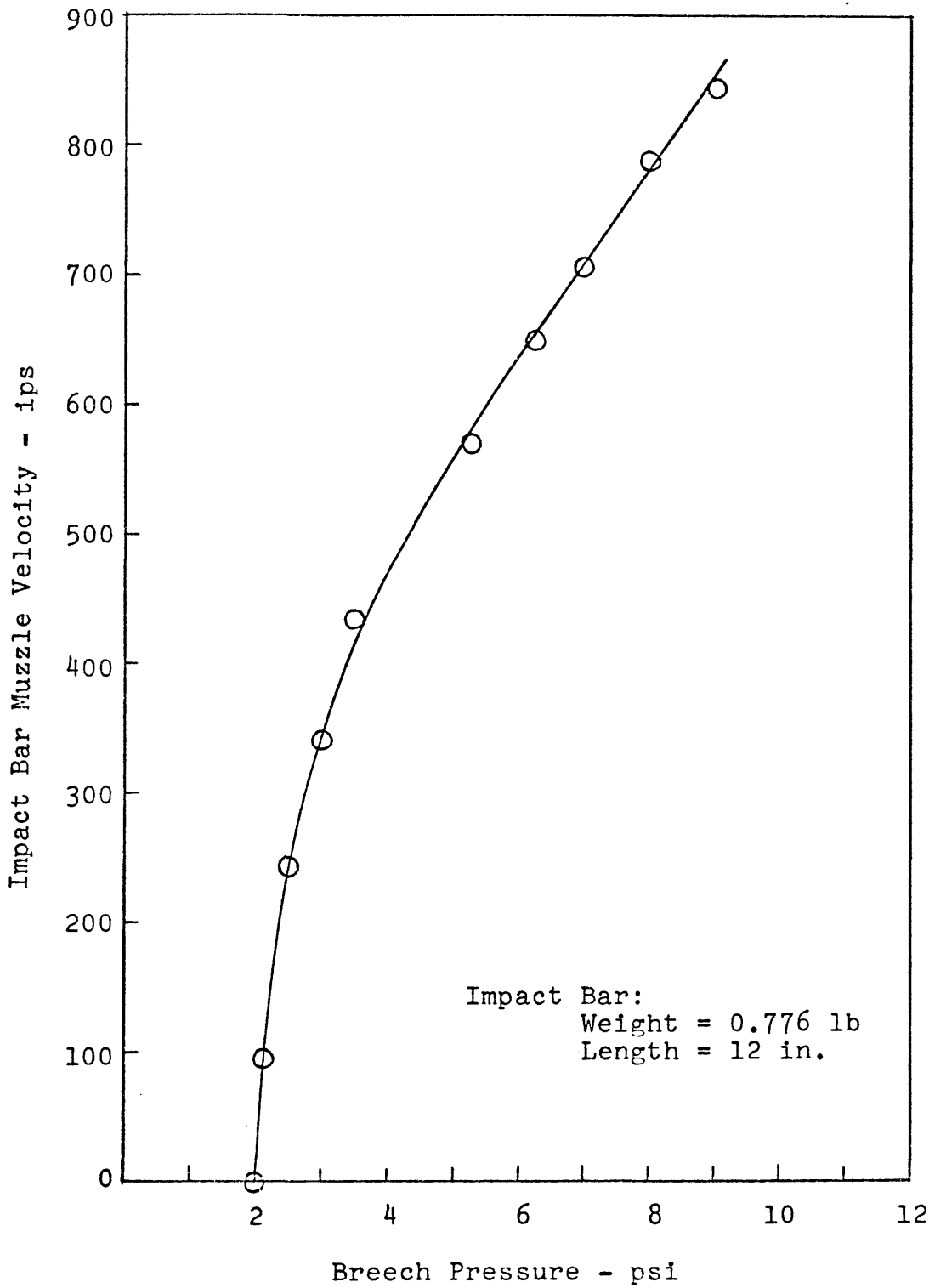


Figure 7. Impact Bar Muzzle Velocity Versus Air Gun Breech Pressure.

Velocity Measuring Equipment

The velocities of the bars before and after impact were measured with a drum camera which photographed the displacement of the ends of the bars within a calibrated time scale. A typical trace for a plastic test is shown in Fig. 8. The horizontal lines marked f are images of the camera slit illuminated by a stroboscope which flashed at 4 msec intervals thereby calibrating the time base. The line bc represents the end of the specimen bar at rest. The impact bar enters the field of view at point a and travels along the path ac until it impacts at point c. The impact velocity was determined from the slope of line ac. The distance cd represents the time the impact bar and specimen bar are in contact. The velocity of the impact bar after impact is represented by line de while dg represents the specimen bar velocity after impact.

The drum camera consisted of an 8 in. diam wooden drum, a light proof box containing a 0.0001 in. slit, an AC motor with variable speeds up to 4000 rpm, and a standard f 6.8 commercial lens with a 65 mm focal length. The camera was positioned to give a magnification ratio of 1.0. The shutter actuating lever was connected to a 0.006 in. diam iron trip wire which passed through the ports in the barrel of the air gun 9 1/2 in. away from the end of the specimen bar. A

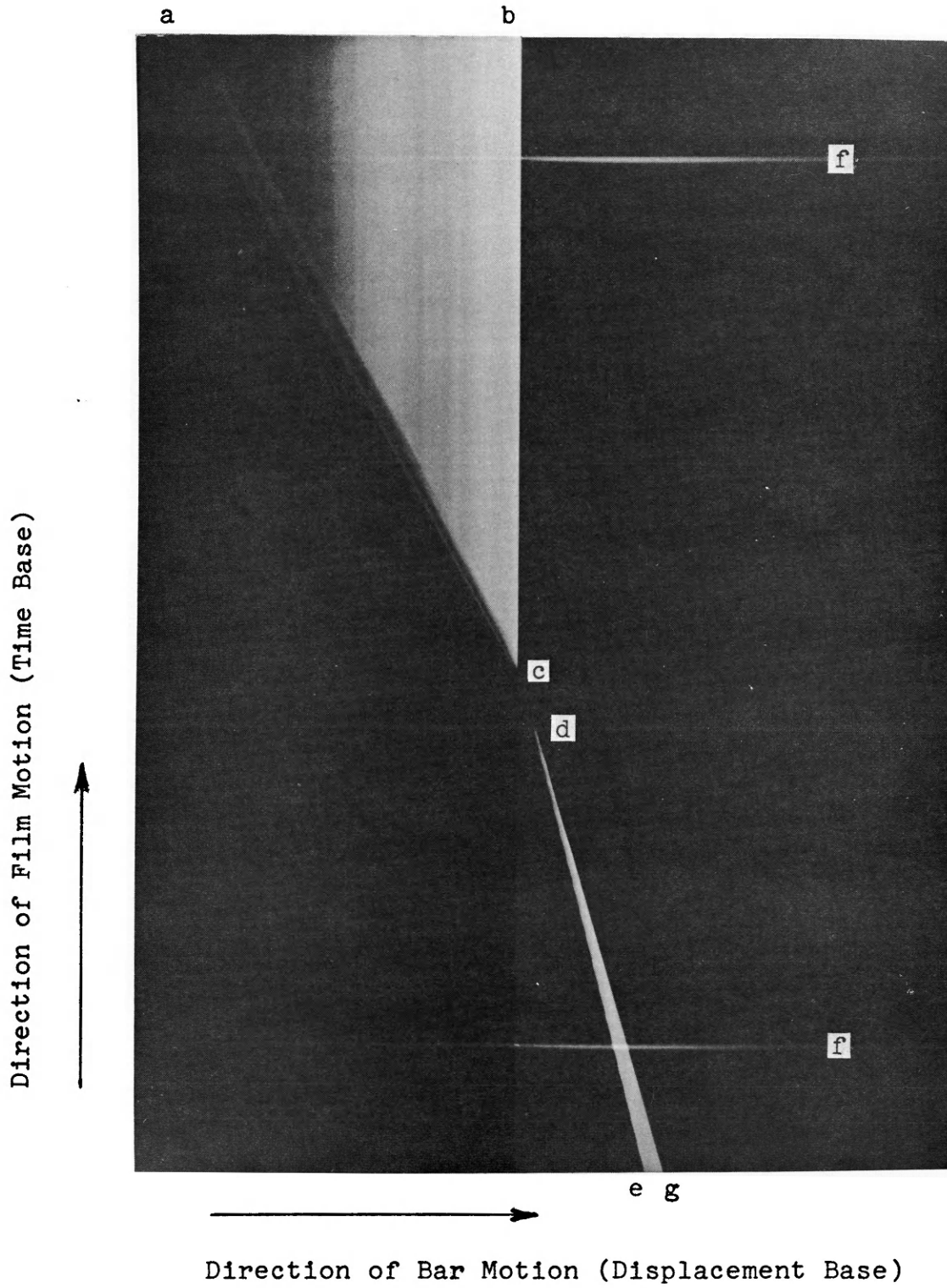


Figure 8.

Drum Camera Trace
(Test P-18)

shutter speed of 1/25 sec was determined to be enough time for the camera to record the whole impact sequence for the slowest impact velocity used. The speed of the drum camera was set at 1,500 rpm so that only one revolution of the film would occur during the time the shutter was open. The film used was 70 mm Kodak Royal Pan SP-473. A 150 w projector flood lamp was used as a light source, the beam of which passed through collimator plates before reaching the impact plane. The stroboscope used was a General Radio Strobotac type 1531-A which was set at 15,000 flashes/min so that there would be 10 timing lines on the film.

Vibration Measuring Equipment

Lateral Strain Measuring Circuit

Four BLH semiconductor strain gauges (SPB1-12-12) were mounted longitudinally on the specimen bar 90 degrees apart. The side gauges were placed in adjacent arms of a wheatstone bridge circuit to measure the horizontal component of the lateral vibrations and the top and bottom gauges were placed in adjacent arms of a second wheatstone bridge circuit to measure the vertical component of the lateral vibrations. Placing the gauges in adjacent arms of the wheatstone bridge allows their outputs to be subtracted electrically. Since both gauges in each bridge are 180 degrees apart, each experiences the same bending strain but of opposite sign so that

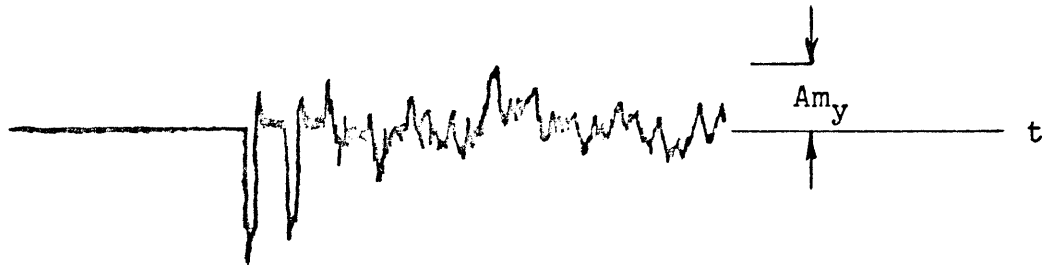
the circuit output is twice the bending strain output for each gauge. The longitudinal compressive strain in both gauges effectively cancel one another. The circuit output for each bridge went to an oscilloscope equipped with a Polaroid camera that used 3000 speed/type 47 film. A sketch of a typical horizontal and vertical lateral strain trace is shown in Fig. 9. The lateral strain amplitude is taken as half the maximum total strain range.

Longitudinal Strain Measuring Circuit

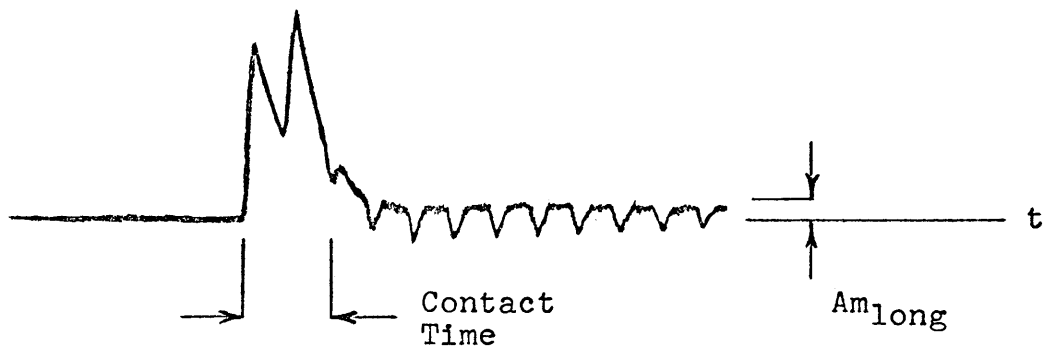
Provision was made so that the top and bottom gauges on the specimen bar could also be placed in series in one arm of a wheatstone bridge to measure the longitudinal vibrations. Placing the gauges in series allows their outputs to be added and averaged electrically so that the circuit output gives the true longitudinal compressive strain and eliminates all the strain indication due to bending. Fig. 9 shows a representative longitudinal strain trace. The longitudinal strain amplitude is taken as the highest peak after the initial loading pulse (or pulses). If $2\Delta V < V_0 < 4\Delta V$ there will only be one loading pulse representing the elastic strain in the bars during plastic deformation of the specimen. If $4\Delta V < V_0 < 6\Delta V$ there will be a second loading pulse in the bars before separation but since both ends of the specimen have the same velocity there is no further plastic straining.



Lateral Vibration Trace X
(Test P-21)



Lateral Vibration Trace Y
(Test P-21)



Longitudinal Vibration Trace
(Test P-19)

Figure 9. Traces of Typical Strain Gauge Signals.

The longitudinal strain amplitude as measured from oscilloscope traces may be related to the longitudinal strain by means of the wheatstone bridge circuit geometry as shown in Fig. 10. The current through the gauges (I_g) is related to the applied circuit voltage (V) by

$$I_g = \frac{V}{R_g + R} \quad (64)$$

where R_g is the series gauge resistance and R is a matching resistance. Also, at any instant in this circuit

$$V_g = I_g R_g \quad (65)$$

where V_g is the voltage across the gauges. Substituting Eq. (64) into Eq. (65) we have

$$V_g = \frac{R_g}{R_g + R} V \quad (66)$$

To find a relationship between dV_g (change in voltage across gauges due to change in strain) and dR_g (change in series gauge resistance due to change in strain) Eq. (66) is differentiated with respect to R_g :

$$dV_g = \frac{(R_g + R)dR_g - R_g dR_g}{(R_g + R)^2} V = \frac{VR dR_g}{(R_g + R)^2} \quad (67)$$

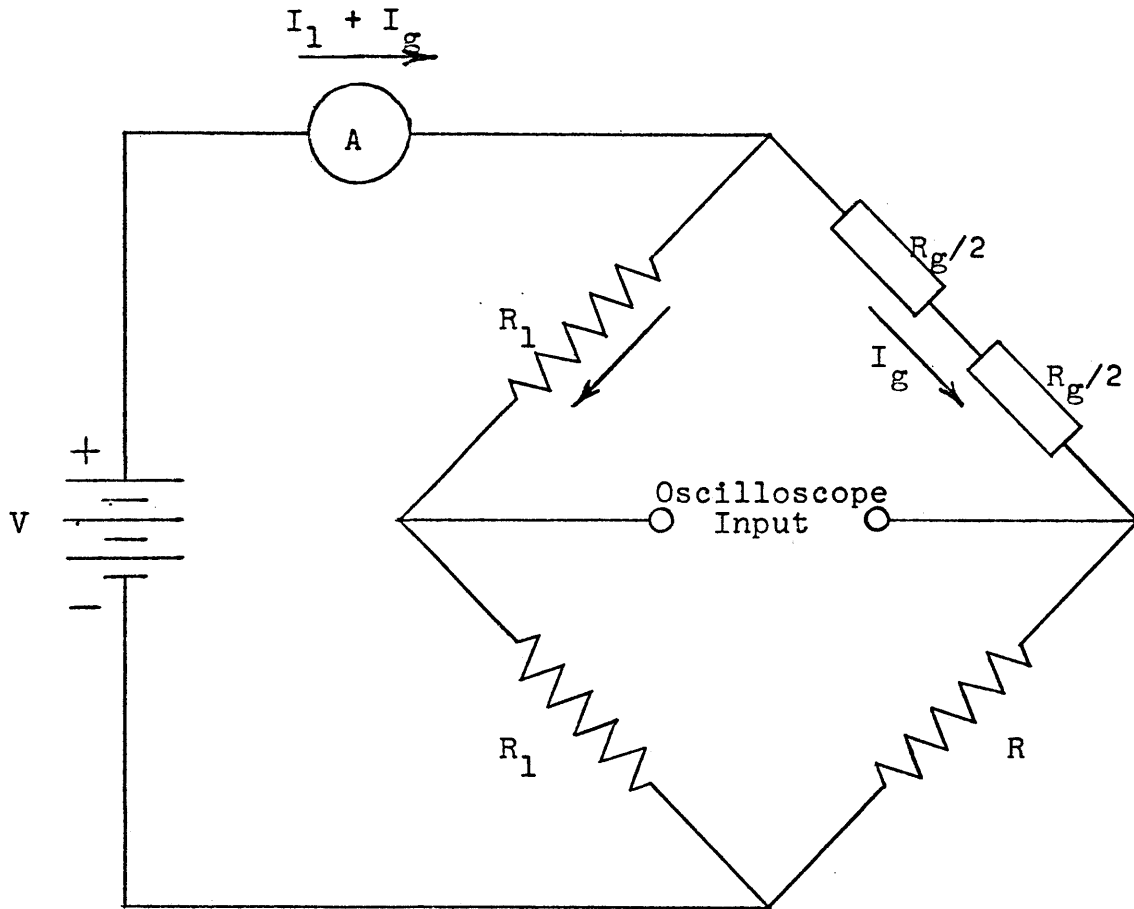


Figure 10. Wheatstone Bridge Circuit for Measuring Longitudinal Vibrations

Multiplying and dividing the right side of Eq. (67) by R_g gives

$$dV_g = \frac{VRR_g}{(R_g + R)^2} \frac{dR_g}{R_g} \quad . \quad (68)$$

But by definition of gauge factor (K_g),

$$K_g = \frac{dR_g}{R_g} \frac{1}{de} \quad (69)$$

where de is the change in strain applied to the gauge. Substituting Eq. (69) into Eq. (68) we have

$$dV_g = \frac{VRR_g}{(R_g + R)^2} K_g de \quad . \quad (70)$$

Substituting for $\frac{V}{R_g + R}$ its value as given in Eq. (64)

$$dV_g = \frac{RR_g}{R_g + R} I_g K_g de \quad . \quad (71)$$

And since $R_g = R$ we have

$$dV_g = \frac{1}{2} I_g R K_g de \quad . \quad (72)$$

Rewriting Eq. (72) for strain

$$de = \frac{2 dV_g}{I_g R K_g} \quad . \quad (73)$$

But $de = e_{\text{long}}$ since the initial strain is zero and

$dV_g = (VS) Am_{long}$ where VS is the vertical sensitivity of the oscilloscope (volts/cm) and Am_{long} is the longitudinal strain amplitude (cm). Therefore Eq. (73) becomes

$$e_{long} = \frac{2 (VS) Am_{long}}{I_g R_g K_g} \quad (74)$$

which is Eq. (44) used in determining longitudinal vibration energy loss.

Oscilloscope Sweep Triggering Circuit

An oscilloscope sweep speed of 0.2 msec/cm was used in all tests since it was of the same order of magnitude as the time (119 μ sec) it would take for a stress wave to make a round-trip traverse in the 12 in. long elastic bar. It was necessary to start this sweep at precisely the right instant so that the trace would show the complete impact sequence as well as a 3 cm (625 μ sec) impact delay in 10 cm of screen. Thus the oscilloscope was triggered when the impact bar was at a set distance (trip distance) from the specimen bar. The trip distance varied directly with the impact velocity: for instance when $V_o = 200$ ips the trip distance was 1/8 in. and when $V_o = 600$ ips the trip distance was 3/8 in.

The photocell circuit shown in Fig. 11, containing a N-P-N silicon photocell placed behind the drum camera objective lens, was used to trigger the oscilloscope sweep at the

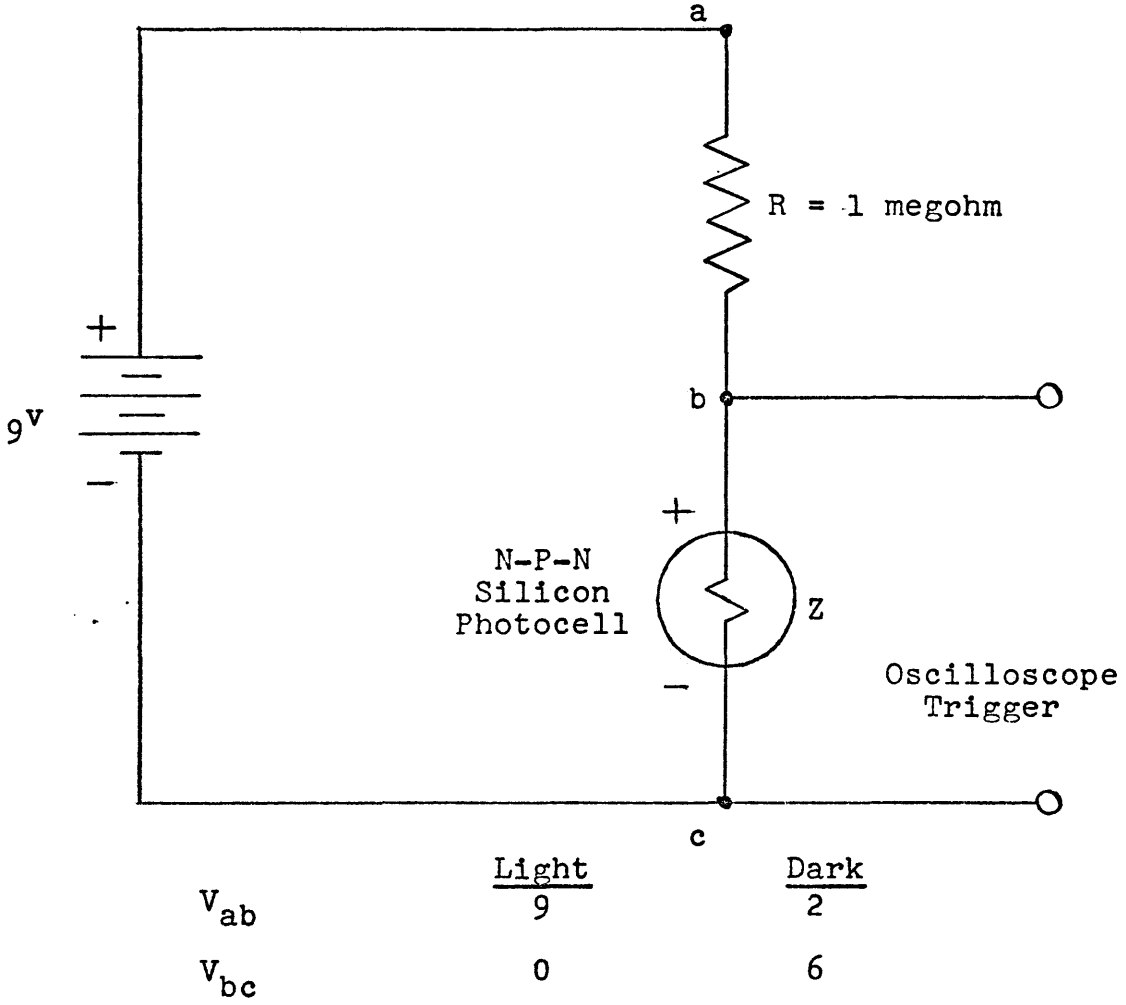


Figure 11. Oscilloscope Sweep Triggering Circuit.

prescribed trip distance. The resistance (R) was chosen such that the impedance (Z) of the photocell would be much less than R in light and much greater than R in dark. Thus, for an applied circuit voltage of 9 volts the voltage across the photocell (V_{bc}) gradually changed from zero volts at maximum illumination when the bars were 1 in. apart to 6 volts at minimum illumination when the bars were in contact. The trigger level on the oscilloscope was set for a positive voltage change between zero and 6 volts corresponding to a given trip distance.

Plastic Strain Measuring Equipment

The diameter of the specimen was measured at intervals along the specimen axis by two 0.0001 in. dial gauges. The specimen was mounted on a v-grooved engravers table that could be moved by micrometer lead screws in the longitudinal, vertical, or transverse direction.

EXPERIMENTAL PROCEDURE

1. Measure initial specimen dimensions.
2. Glue or screw specimen on bar.
3. Record weight of impact bar and specimen bar.
4. Check A1 spacer position on impact bar.
5. Check air bearing - barrel alignment.
6. Check slit image and record displacement magnification.
7. Check stroboscope calibration.
8. Check and record drum camera speed.
9. Position stroboscope and record time base.
10. Check oscilloscope sweep triggering circuit - Record trip distance.
11. Drive impact bar to breech of barrel following steps a and b of firing sequence.
12. Load and position drum camera.
13. Position specimen bar in air bearings.
14. Set catcher in place and tighten mounting bolts.

15. Set bridge circuit current and balance bridge for appropriate oscilloscope traces.
16. Record oscilloscope settings and check Polaroid camera.
17. Set mechanical trip wire and cock drum camera shutter.
18. Cock air gun trigger and set breech pressure following steps c through f of firing sequence.
19. Turn on drum camera motor, stroboscope, and photo-flood.
20. Heat specimen with induction coil (remove coil).
21. Set air bearing pressure to 40 psi.
22. Open Polaroid camera shutter.
23. Fire gun when drum camera reaches terminal velocity following steps g through i of firing sequence.
24. Close Polaroid camera shutter.
25. Develop oscilloscope trace pictures.
26. Reset gun for next test according to step j of firing sequence.
27. Develop drum camera film.
28. Measure final specimen dimensions.

EXPERIMENTAL RESULTS AND DISCUSSION

The dynamic flow stress for copper was determined for temperatures of 75°F and 475°F over the strain rate range $10^2 - 10^3 \text{ sec}^{-1}$. These tests are compared with the results of other investigators by the ratio of dynamic stress increase to static stress ($S_p - S_o/S_o$) for a given strain and strain rate.

Tests at 75°F

The experimental data and results for the 75°F tests are given in Tables 3 and 4, Appendix III. Only those tests for which the momentum balance was 97% or greater are reported. A summary of the test results is given in Table 5. These are averaged values for each strain rate level.

Table 5. Summary of 75°F Results

$\dot{\epsilon}$ sec ⁻¹	Momentum Balance (%)	ϵ_a^*	S_p psi	S_o psi	Stress Increase Ratio $S_p - S_o / S_o$
278	98.5	0.0335	60,800	47,200	0.29
752	98.8	0.0936	67,700	47,200	0.43
1123	98.1	0.1470	70,300	47,200	0.49

These results are compared with the results of other investigators in Fig. 12. The "filled points" represent stress increase ratios for various investigators that have a uniform strain profile in the specimen, a uniaxial state of stress, and a plastic strain level of 0.40 to 0.75. The "open points" represent specimen strain profiles ranging from uniform to highly non-uniform, states of stress ranging from uniaxial to triaxial, and plastic strains ranging from 0.04 to 0.25. The data of Lindholm (1965) only differed from the author's work with respect to strain level ($\epsilon = 0.06$) so it was cross plotted and extrapolated to a similar state of work hardening (i.e. to the same static flow stress) to permit comparison. It is interesting to note that this

* The actual plastic strain level in the specimens is the sum of ϵ_a and the initial strain of 0.60 in the cold-worked copper.

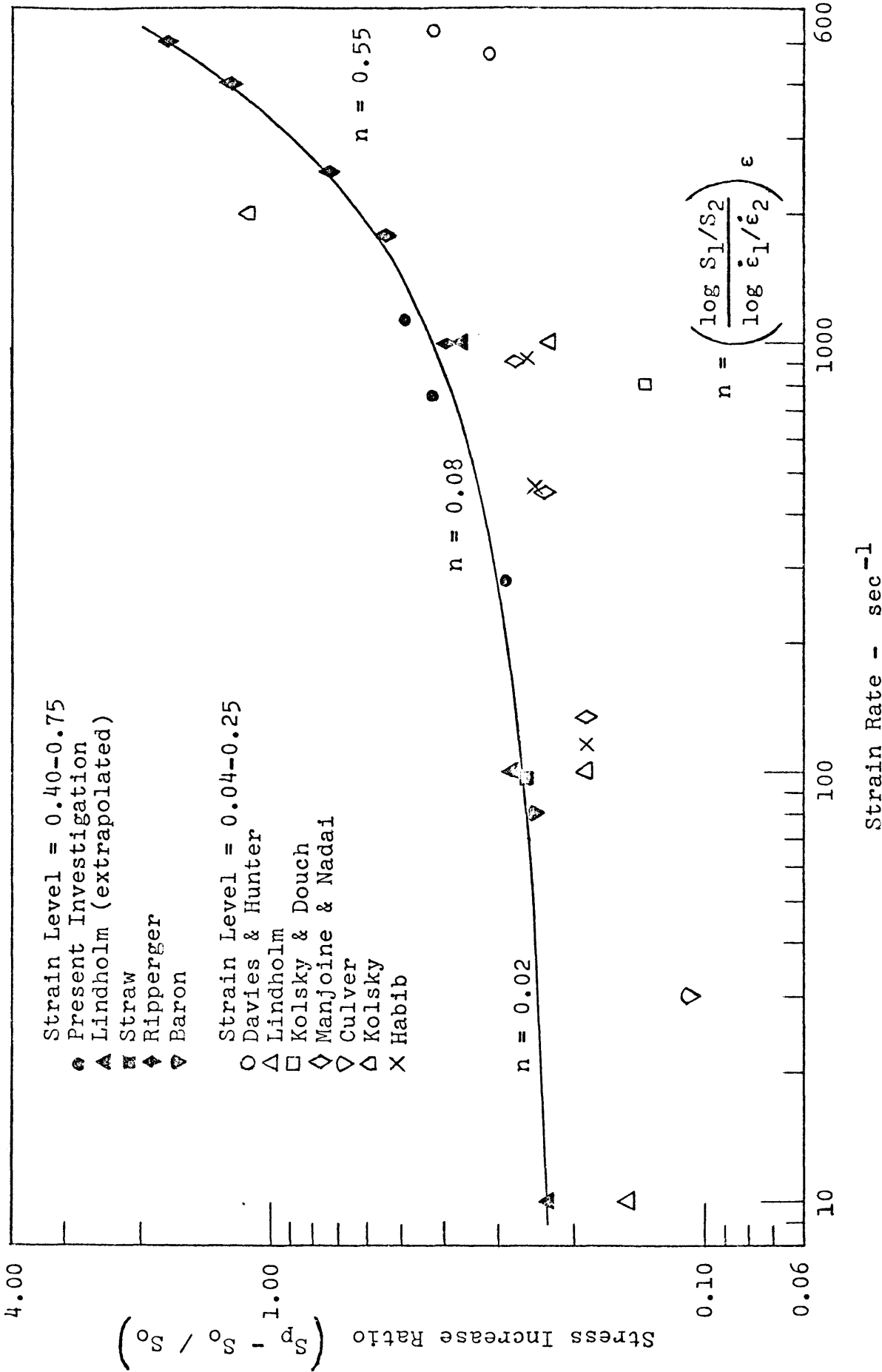


Figure 12. Stress Increase Ratio Versus Strain Rate for Copper at Room Temperature.

extrapolated data falls on the trend line at a strain rate of 100 sec^{-1} . This indicates that the state of stress and strain in two different tests must be identical before the results can be meaningfully compared.

The general trend line indicates that rate sensitivity (n) increases nonlinearly from a value of 0.02 in the strain range $10 - 100 \text{ sec}^{-1}$ to a value of 0.55 in the strain rate range $2000 - 5000 \text{ sec}^{-1}$. The author's data shows a rate sensitivity of 0.10 in the strain rate range $200 - 1200 \text{ sec}^{-1}$ which is reasonably close to the general trend value of 0.08. A rate sensitivity of 0.10 corresponds to a 26% increase in stress for a factor of 10 increase in strain rate.

Tests at 475°F

The experimental data and results for the 475°F tests are given in Tables 6 and 7, Appendix IV. Recrystallization of the copper occurred during heating so that before a correct estimate of rate sensitivity could be made strain hardening was accounted for as shown in Appendix V. A summary of the test results is given in Tables 8 and 9.

Table 8. Summary of 475°F Results Neglecting Strain Hardening

$\dot{\epsilon}$ sec ⁻¹	Momentum Balance (%)	ϵ_a	S_p psi	S_o psi	Stress Increase Ratio $S_p - S_o / S_o$
582	97.9	0.0763	27,000	-	-
932	99.1	0.1235	34,400	-	-

Table 9. Summary of 475°F Results Accounting for Strain Hardening

$\dot{\epsilon}$ sec ⁻¹	Momentum Balance (%)	ϵ_a	S_p psi	S_o psi	Stress Increase Ratio $S_p - S_o / S_o$
582	97.9	0.0400	29,000	19,600	0.48
932	99.1	0.0400	32,400	19,600	0.65

These results are shown graphically in Fig. 13. The apparent rate sensitivity for copper in the strain rate range 200 - 1200 sec⁻¹ is 0.52 if strain hardening is neglected. Correcting for strain hardening shows the true rate sensitivity for recrystallized copper to be 0.24 corresponding to a 73% increase in stress for a factor of 10 increase in strain rate. This rate sensitivity is an

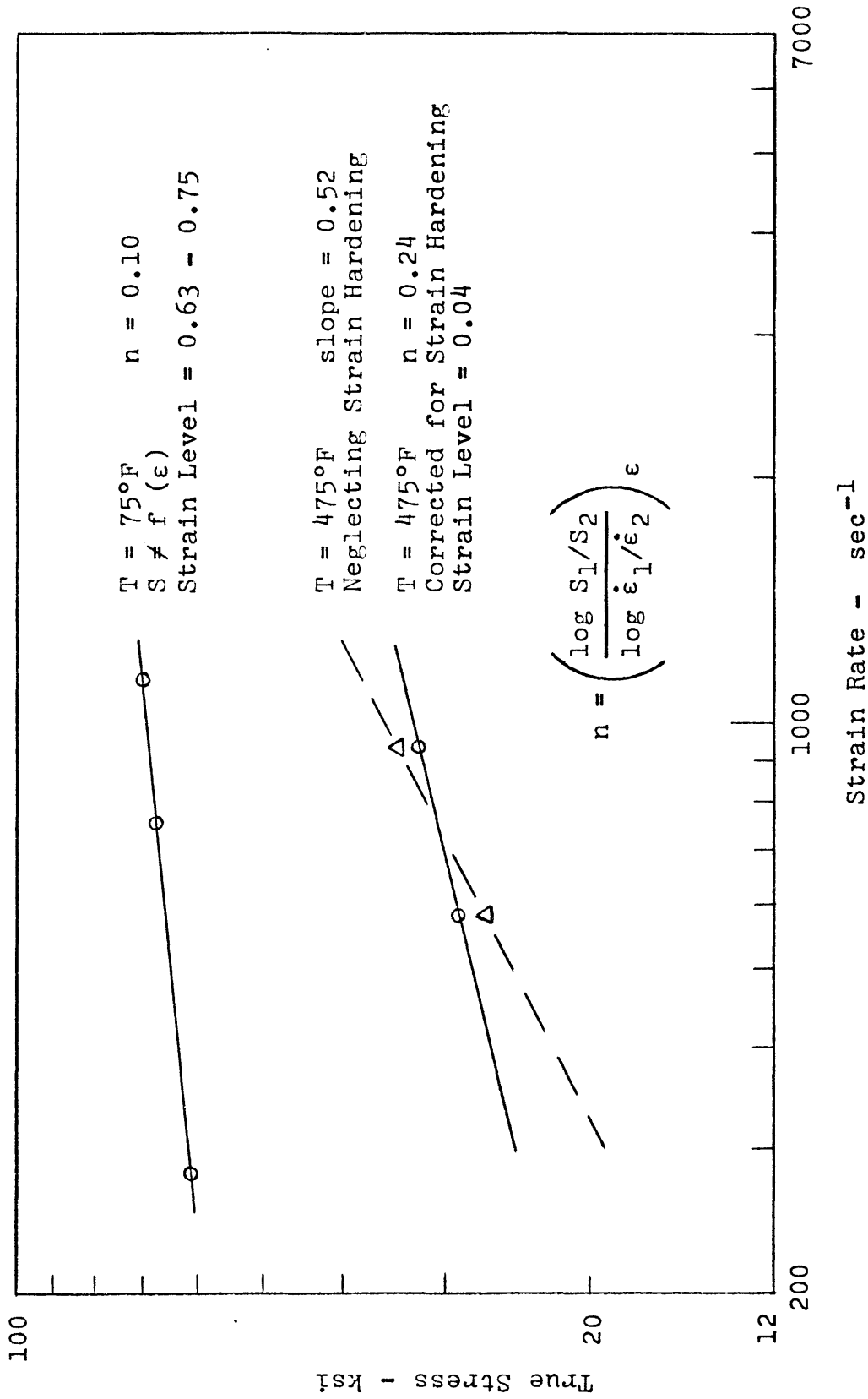


Figure 13. True Stress Versus Strain Rate for Copper at 475°F.

increase of 2.4 times the room temperature value for cold-worked copper. However, in comparing the rate sensitivities at the two temperatures note must be taken of the fact that the strain levels are different.

CONCLUSIONS

1. Rate sensitivity increases with increasing strain rate; at 75°F and at a plastic strain level of 0.40 - 0.75 the rate sensitivity for copper increased from a value of 0.02 in the strain rate range 10 - 100 sec⁻¹ to a value of 0.55 in the strain rate range 2000 - 5000 sec⁻¹.
2. Recrystallization occurred during heating at 475°F; if the strain hardening that took place during subsequent deformation had been neglected the apparent rate sensitivity for copper would have been incorrectly higher by a factor of 2.
3. Rate sensitivity apparently increases with increasing temperature;* in the strain rate range 200 - 1200 sec⁻¹ the rate sensitivity for cold-worked copper was 0.10 at 75°F corresponding to a 26% increase in stress for a

*Note must be taken of the fact that the strain levels were different at the two temperatures.

factor of 10 increase in rate, while at 475°F the rate sensitivity for recrystallized copper was 0.24 corresponding to a 73% increase in stress for a factor of 10 increase in rate.

4. For a combination of high strain rate (2000 - 5000 sec⁻¹) and high temperature (475°F) it is expected that the rate sensitivity will approach a limiting value of unity corresponding to viscous flow where stress is proportional to strain rate.

APPENDIX I

Tabulated Room Temperature Results of Previous Investigators

INVESTIGATOR	Straw (1965)	Bell & Werner (1962)
MATERIAL	cold-worked copper	annealed copper
TEST TYPE	bar-bar compression	bar-bar compression
ENERGY SOURCE	ballistic pendulum	air gun
LOAD MEASUREMENT	from plastic de- formation energy determined by energy balance	calculated from displacement-time curve for elastic bar
STRAIN MEASUREMENT	from final specimen diameter	from diffraction grating on gauge length
DYNAMIC STRAIN RATE	96 sec ⁻¹	250 sec ⁻¹
STRESS INCREASE RATIO $S_p - S_o / S_o$	0.26	0
SPECIMEN L/D RATIO	2.00	10.10
STRAIN LEVEL	0.70	0.02

Tabulated Room Temperature Results of Previous Investigators

(continued)

INVESTIGATOR	Ripperger (1965)	Lindholm (1965)
MATERIAL	cold-worked copper	annealed copper
TEST TYPE	bar-bar compression	bar-bar compression
ENERGY SOURCE	air gun	explosively driven striker bar
LOAD MEASUREMENT	from stress-time curve using quartz crystal as stress transducer	from pressure- time histories in elastic pressure bars
STRAIN MEASUREMENT	from strain-time curve using etched- foil strain gauges on specimen	from strain-time histories in elastic pressure bars using resistance strain gauges
DYNAMIC STRAIN RATE	1000,1750,2500, 4000,5000 sec ⁻¹	10,100,1000 sec ⁻¹
STRESS INCREASE RATIO $S_p - S_o / S_o$	0.40, 0.55, 0.75, 1.28, 1.76	0.15, 0.19, 0.23
SPECIMEN L/D RATIO	2.00	unknown
STRAIN LEVEL	0.62	0.06

Tabulated Room Temperature Results of Previous Investigators

(continued)

INVESTIGATOR	Kolsky & Douch (1962)	Kolsky (1949)
MATERIAL.	annealed copper	annealed copper
TEST TYPE	bar-bar compression	bar-bar compression
ENERGY SOURCE	air gun	explosive detonation
LOAD MEASUREMENT	from elastic stress pulse in steel pressure bar	from parallel plate condenser microphone measuring dis- placement of elastic bar
STRAIN MEASUREMENT	from final diameter measurements taken at inter- vals along specimen length	from cylindrical condenser micro- phone measuring amplitude of pressure pulse
DYNAMIC STRAIN RATE	800 sec ⁻¹	2000 sec ⁻¹
STRESS INCREASE RATIO $S_p - S_o / S_o$	0.14	1.13
SPECIMEN L/D RATIO	8.00	0.02
STRAIN LEVEL	0.06	0.04

Tabulated Room Temperature Results of Previous Investigators

(continued)

INVESTIGATOR	Davies & Hunter (1963)	Habib (1948)
MATERIAL	annealed copper	annealed copper
TEST TYPE	bar-bar compression	bar-block compression
ENERGY SOURCE	explosive detonation	air gun
LOAD MEASUREMENT	from parallel plate condenser microphone measuring dis- placement of elastic bar	from numerical dif- ferentiation of curves of plastic deformation energy versus deformation obtained by energy balance
STRAIN MEASUREMENT	from displace- ment-time curves of elastic bar with and without specimen	from final length of specimen
DYNAMIC STRAIN RATE	5,300, 4,700 sec ⁻¹	115, 460, 920 sec ⁻¹
STRESS INCREASE RATIO $S_p - S_o / S_o$	0.43, 0.32	0.19, 0.25, 0.26
SPECIMEN L/D RATIO	0.31, 0.51	1.54
STRAIN LEVEL	0.08	0.25

Tabulated Room Temperature Results of Previous Investigators

(continued)

INVESTIGATOR	Baron (1956)	Manjoine & Nadai (1940)
MATERIAL	annealed copper	annealed copper
TEST TYPE	block-block tension	block-block tension
ENERGY SOURCE	charpy pendulum	flywheel
LOAD MEASUREMENT	from weigh-bar with strain gauges	from elastic strain in a rigid steel bar
STRAIN MEASUREMENT	calculated from force-time curve	from relative motion between both ends of the specimen
DYNAMIC STRAIN RATE	80 sec ⁻¹	135, 450, 900 sec ⁻¹
STRESS INCREASE RATIO $S_p - S_o / S_o$	0.25	0.19, 0.24, 0.28
SPECIMEN L/D RATIO	6.00	5.50
STRAIN LEVEL	0.40	0.20

Tabulated Room Temperature Results of Previous Investigators

(continued)

INVESTIGATOR	Culver (1963)
MATERIAL	annealed copper
TEST TYPE	bar-block tension
ENERGY SOURCE	spring
LOAD MEASUREMENT	from strain gauge dynamometer
STRAIN MEASUREMENT	from drum camera trace of the motion of scribed lines on specimen
DYNAMIC STRAIN RATE	30 sec ⁻¹
STRESS INCREASE RATIO $S_p - S_o / S_o$	0.11
SPECIMEN L/D RATIO	5.00
STRAIN LEVEL	0.10

APPENDIX II

Elastic Calibration Data

Table 1. Measured Elastic Calibration Data - $V_0 = 2\Delta V$

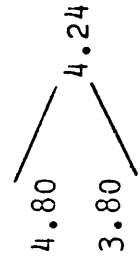
Test No.	V_0 ips	V_1 ips	V_s ips	A_{m_x} cm	A_{m_y} cm	$A_{m_{lat}}^2$ cm ²	$A_{m_{long}}$ cm	$A_{m_{long}}^2$ cm ²
E-1	227.9	0	222.7	-	-	-	0.29	
E-2	251.4	0	245.4	-	-	-	0.31	
E-3	246.9	0	239.6	-	-	-	0.28	0.084*
E-4	233.0	0	230.3	-	-	-	0.28	
E-6	253.6	0	246.8	0.61	0.69	0.85	-	0.084
E-7	244.5	0	233.4	0.71	0.78	1.10	-	0.084
E-8	236.5	0	230.0	0.51	0.74	0.81	-	0.084
E-10	243.3	0	233.9	0.59	0.82	1.02	-	0.084

Bar Weights: impact bar = 0.776 lb
specimen bar = 0.776 lb

*This value is used in all subsequent elastic tests where only lateral vibrations are measured.

Table 2. Calculated Elastic Calibration Data - $V_0 = 2 \Delta V$

Test No.	Momentum Balance %	KE ₀ in-lb	KE _i in-lb	KE _s in-lb	E _v in-lb	E _{long} in-lb	E _{lat} in-lb	K in-lb/cm ²
E-6	97.3	64.7	0	61.3	3.4	0.02	3.38	3.97
E-7	95.5	60.1	0	54.8	5.3	0.02	5.28	4.80
E-8	97.3	56.3	0	53.2	3.1	0.02	3.08	3.80
E-10	96.1	59.5	0	55.0	4.5	0.02	4.48	4.39



$$E_{lat} = 4.24 \text{ Am}_{lat}^2$$

APPENDIX III

75°F Experimental Data

Table 3. 75°F Measured Data

Test No.	V _o ips	V _i ips	V _s ips	A _{m,x} cm	A _{m,y} cm	A _{m,lat} cm ²	L _o in.	D _o in.	D _{avg} in.
P-14	344.3	158.3	184.7	0.99	1.09	2.17	0.5019	0.2508	0.2551
P-16	338.1	150.9	180.6	0.71	1.16	1.85	0.5009	0.2512	0.2555
P-18	339.9	153.9	179.2	1.05	1.22	2.59	0.5009	0.2501	0.2542
P-19	569.7	229.0	332.5	0.85	0.78	1.33	0.5004	0.2518	0.2637
P-20	553.8	225.7	326.8	0.60	0.71	0.86	0.5008	0.2506	0.2620
P-21	590.4	235.5	342.9	0.82	0.85	1.39	0.4999	0.2520	0.2648
P-22	702.2	313.1	376.0	0.67	0.67	0.90	0.4996	0.2509	0.2694
P-25	711.5	315.5	384.4	0.58	0.71	0.84	0.4996	0.2509	0.2705
P-26	708.2	311.8	381.6	0.63	0.69	0.87	0.5001	0.2507	0.2700

L_B = 12 in.

Bar Weights:

c_o = 16,800 fps

impact bar = 0.776 lb

ρ = 7.35 x 10⁻⁴ lb-sec/in⁴

specimen bar = 0.776 lb

A_p/A = 1/4

Table 4. 75°F Calculated Data

Test No.	Momentum Balance %	KE _O in-lb	KE _I in-lb	KE _S in-lb	E _V in-lb	E _P in-lb	ϵ_a	vol in ³	S _p psi
P-14	99.6	119.2	25.2	34.3	9.2	50.5	0.03394	0.02478	60,000
P-16	98.0	115.0	22.9	32.8	7.8	51.5	0.03394	0.02481	61,200
P-18	98.0	116.2	23.8	32.3	11.0	49.1	0.03254	0.02460	61,300
P-19	98.6	326.5	52.8	111.2	5.6	156.9	0.09250	0.02491	68,000
P-20	99.8	308.5	51.2	107.4	3.7	146.2	0.08900	0.02469	66,400
P-21	98.0	350.6	55.8	118.3	5.9	170.6	0.09920	0.02492	68,900
P-22	98.1	496.0	98.6	142.2	3.8	251.4	0.14220	0.02469	71,600
P-25	98.4	509.2	100.1	148.6	3.6	256.9	0.15040	0.02469	69,200
P-26	97.9	504.5	97.8	146.5	3.7	256.5	0.14840	0.02467	70,100

Table 4. 75°F Calculated Data (continued)

Test No.	S _p psi	ΔV ips	$\frac{V_o}{\Delta V}$	$\dot{\epsilon}_1$ sec ⁻¹	$\dot{\epsilon}_2$ sec ⁻¹	$\dot{\epsilon}_{avg}$ sec ⁻¹	$\frac{S_p - S_o}{S_o}$
P-14	60,000	101.2	3.40	288	285	287	0.27
P-16	61,200	103.2	3.28	267	285	276	0.30
P-18.	61,300	103.4	3.29	270	273	272	0.30
P-19	68,000	114.7	4.97	711	777	744	0.44
P-20	66,400	112.0	4.94	688	748	718	0.41
P-21	68,900	116.2	5.08	752	834	793	0.46
P-22	71,600	120.8	5.81	987	1195	1091	0.52
P-25	69,200	116.7	6.10	1029	1264	1147	0.47
P-26	70,100	118.2	5.99	1013	1247	1130	0.49

$$\dot{\epsilon}_1 = \frac{2(V_o - 2\Delta V)}{L_o + L_o \ln^{-1} \epsilon_a}$$

$$\dot{\epsilon}_2 = \frac{\epsilon_a c_o}{2L_B}$$

$$S_o = 47,200 \text{ psi}$$

APPENDIX IV

475°F Experimental Data

Table 6. 475°F Measured Data

Test No.	V _o ips	V _i ips	V _s ips	A _m x cm	A _m y cm	A _m ² _{lat} cm ²	L _o in.	D _o in.	D _{avg} in.
P-41	594.6	254.2	326.1	0.84	0.64	1.11	0.7468	0.3742	0.3894
P-42	588.4	252.3	330.4	0.54	0.68	0.75	0.7390	0.3754	0.3902
P-44	556.2	234.3	305.8	0.58	0.50	0.59	0.7498	0.3768	0.3906
P-46	844.9	371.3	461.2	1.35	0.63	2.22	0.7493	0.3754	0.3992
P-47	840.1	371.4	465.3	0.86	1.06	1.86	0.7486	0.3760	0.3998
P-48	848.8	386.5	454.9	0.95	1.06	2.03	0.7497	0.3758	0.4000

L_B = 12 in.c_o = 16,800 fpsρ = 7.35 x 10⁻⁴ lb-sec/in⁴A_p/A = 9/16

Bar Weights:

impact bar = 0.776 lb

specimen bar = 0.776 lb

Table 7. 475°F Calculated Data

Test No.	Momentum Balance %	KE _O in-lb	KE _i in-lb	KE _s in-lb	E _y in-lb	E _p in-lb	ε _a	vol in ³	S _p * psi
P-41	97.6	355.7	65.0	107.0	4.7	179.0	0.07960	0.08209	27,400
P-42	99.0	348.3	64.0	109.8	3.2	171.3	0.07730	0.08175	27,100
P-44	97.1	311.2	55.2	94.1	2.5	159.4	0.07190	0.08357	26,500
P-46	98.5	718.1	138.7	214.0	9.4	356.0	0.12310	0.08289	34,900
P-47	99.6	710.0	139.8	217.8	7.9	344.5	0.12270	0.08308	33,800
P-48	99.1	724.8	150.3	208.2	8.6	357.7	0.12480	0.08311	34,500

* Average flow stress neglecting strain hardening - strain hardening accounted for in Appendix V.

Table 7. 475°F Calculated Data (continued)

Test No.	Sp* psi	ΔV ips	$\frac{V_o}{\Delta V}$	$\dot{\epsilon}_1$ sec ⁻¹	$\dot{\epsilon}_2$ sec ⁻¹	$\dot{\epsilon}_{avg1}$ sec	$\frac{Sp-S_o}{S_o}$
P-41	27,400	104.0	5.72	538	669	604	-
P-42	27,100	102.8	5.77	538	650	594	-
P-44	26,500	100.6	5.53	490	604	547	-
P-46	34,900	132.4	6.38	822	1034	928	-
P-47	33,800	128.3	6.55	827	1031	929	-
P-48	34,500	130.9	6.48	832	1049	940	-

$$\dot{\epsilon}_1 = \frac{2(V_o - 2\Delta V)}{L_o + L_o \ln^{-1} \epsilon_a} \quad \dot{\epsilon}_2 = \frac{\epsilon_{aCo}}{2 L_B}$$

* Average flow stress neglecting strain hardening - strain hardening accounted for in Appendix V.

APPENDIX V

Separation of Rate Sensitivity From Strain Hardening at 475°F

The high temperature specimens were impacted when the metal-air surface temperature read 400°F but when the actual interior temperature was 460°F. Assuming 90% of the plastic deformation energy was dissipated in adiabatic heating there was an added temperature rise of 30°F during impact. Thus the average specimen temperature during deformation was 475°F.

A flow stress evaluated from Eq. (37) is valid in the temperature range $75^{\circ}\text{F} < T < 400^{\circ}\text{F}$ where there is no strain hardening. In that temperature range rate sensitivity, defined as the slope of the log stress-log strain rate curve at a fixed value of strain, is also strain independent. For a temperature of 475°F, however, recrystallization has occurred and stress is no longer independent of strain as can be seen in Fig. 14. The nominal recrystallization temperature is 500°F but presumably there is enough scatter in the physical properties due to impurities to start recrystallization at a slightly lower temperature. Thus the flow stress* at 475°F determined from Eq. (37) is only an average stress neglecting strain hardening. It will be

*This average value was used in Appendix IV for estimating an average strain rate ($\dot{\epsilon}_1$) during deformation.

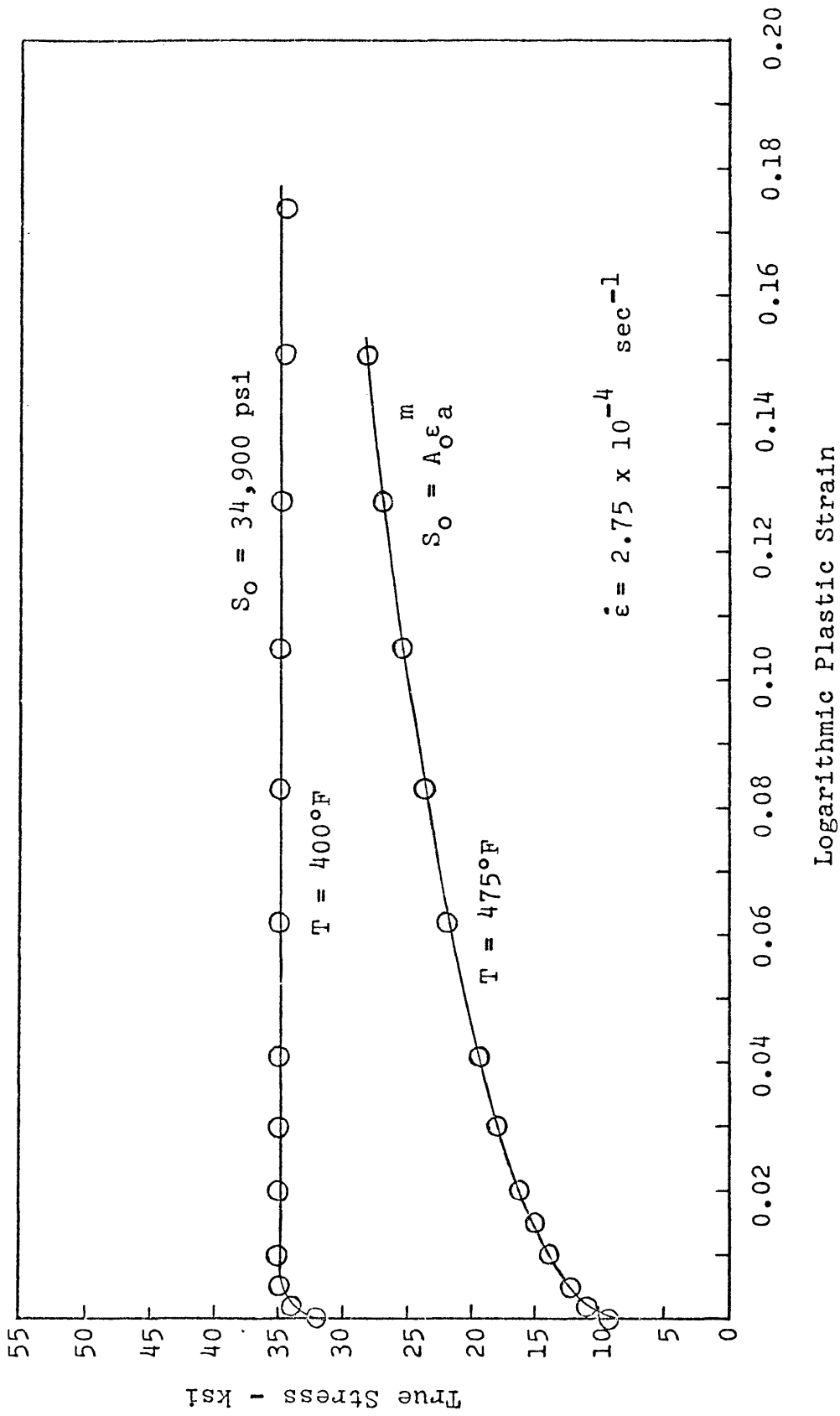


Figure 14. High Temperature Static Stress-Strain Curves for Cold-Worked Copper Exhibiting Strain Hardening.

necessary to determine the dynamic stress-strain curves taking account of strain hardening so that stresses can be compared at the same value of strain.

The stress level, as before from Eq. (36), is dependent on the plastic deformation energy (E_p) as measured from the energy balance and on the total plastic strain (ϵ_a) so that

$$\frac{E_p}{\text{vol}} = \int_0^{\epsilon_a} S_p d\epsilon_a \quad . \quad (75)$$

The static stress-strain behavior is a power function of the form

$$S_o = A_o \epsilon_a^m \quad (76)$$

where m is the strain hardening exponent and A_o is a stress constant at unit strain. The assumption is made that the copper specimen strain hardens at the same rate for both dynamic and static loading so that the dynamic stress-strain relation is

$$S_p = A \epsilon_a^m \quad (77)$$

where A is the stress constant at unit strain for dynamic loading. Substituting Eq. (77) into Eq. (75) we have

$$\frac{E_p}{vol} = \int_0^{\epsilon_a} A \epsilon_a^m d\epsilon_a \quad , \quad (78)$$

integrating

$$\frac{E_p}{vol} = \frac{A \epsilon_a^{m+1}}{m+1} \quad , \quad (79)$$

or

$$A = \frac{E_p}{vol} \frac{m+1}{\epsilon_a^{m+1}} \quad . \quad (80)$$

From the static ($\dot{\epsilon} = 2.75 \times 10^{-4} \text{ sec}^{-1}$) stress-strain curve shown in Fig. 15 m is determined to be 0.27 so that Eq. (80) becomes

$$A = \frac{E_p}{vol} \frac{1.27}{\epsilon_a^{1.27}} \quad . \quad (81)$$

E_p , vol , and ϵ_a have already been evaluated for each test in Appendix IV. Eq. (81) may be used to find A which will govern the stress level of the dynamic curve.

Test No.	$\dot{\epsilon}_{avg}$ sec ⁻¹	E_p/vol in-lb/in ³	ϵ_a	A psi	A_{avg} psi
P-41	604	2,180	0.07960	68,900	
P-42	594	2,095	0.07730	68,900	68,800
P-44	547	1,907	0.07190	68,600	
P-46	928	4,295	0.12310	78,100	
P-47	929	4,147	0.12270	75,700	76,800
P-48	940	4,304	0.12480	76,700	

The dynamic stress-strain curves are shown in Fig. 15. Stresses are compared at a plastic strain of 0.04.

$\dot{\epsilon}$ sec ⁻¹	$(S_p)_{\epsilon=0.04}$ psi	$\frac{S_p - S_o}{S_o}$
2.75×10^{-4}	19,600	0
582	29,000	0.48
932	32,400	0.65

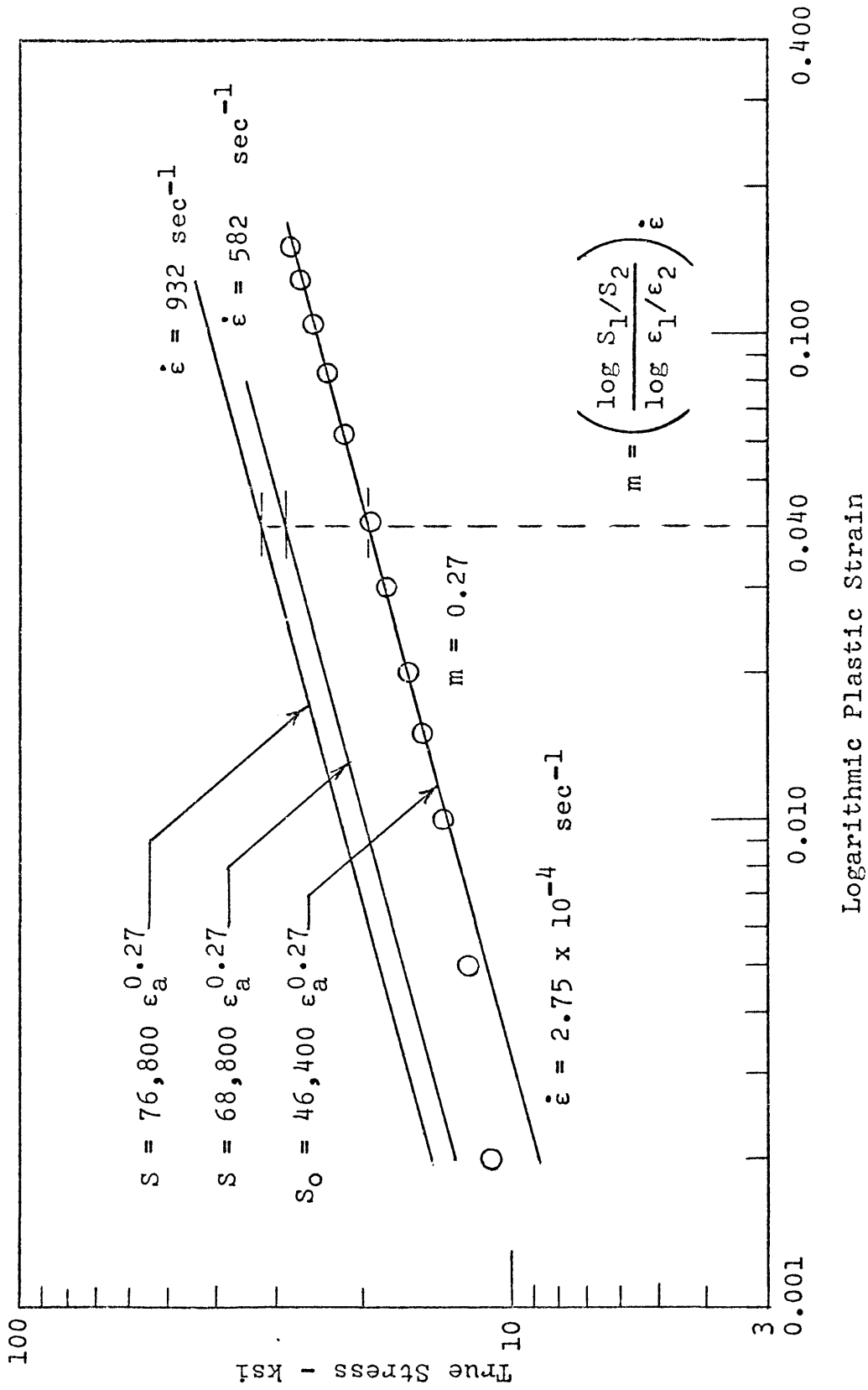


Figure 15. Determination of Strain Hardening Exponent and Stress Constant for Dynamic Tests at 475°F.

LITERATURE CITED

- Baron, H. G., 1956, Stress/strain curves of some metals and alloys at low temperatures and high rates of strain: Jour. Iron Steel Inst., v. 182, part 4, p. 354-365.
- Bell, J. F., and Werner, W. M., 1962, Applicability of Taylor theory of the polycrystalline aggregate to finite wave propagation in annealed copper: Jour. Appl. Physics, v. 33, no. 8, p. 2416-2425.
- Culver, R. S., 1963, An experimental investigation of dynamic deformation phenomenon: Unpublished Doctoral Thesis, University of Cambridge.
- Davies, E. D. H., and Hunter, S. C., 1963, The dynamic compression testing of solids by the method of the split Hopkinson pressure bar: Jour. Mech. Physics Solids, v. 11, p. 155-179.
- Habib, E. T., 1948, A method of making high-speed compression tests on small copper cylinders: Jour. Appl. Mech., v. 15, p. 248-255.
- Kolsky, H., 1949, An investigation of the mechanical properties of materials at very high rates of loading: Phys. Soc. (London) Proc., v. B-62, p. 676-700.
- Kolsky, H., and Douch, L. S., 1962, Experimental studies in plastic wave propagation: Jour. Mech. Physics Solids, v. 10, p. 195-223.
- Lindholm, U. S., 1965, Dynamic deformation of metals: Proc. Colloq. on Behavior of Materials Under Dynamic Loading, ASME, p. 42-61.

Manjoine, M., and Nadai, A., 1940, High-speed tension tests at elevated temperatures: Proc. ASTM, v. 40, p. 822-837.

Ripperger, E. A., 1965, Dynamic plastic behavior of aluminum, copper, and iron: Proc. Colloq. on Behavior of Materials Under Dynamic Loading, ASME, p. 62-80.

Straw, R. L., 1965, Effect of strain rate on flow stress of copper: Unpublished Master of Science Thesis, Colorado School of Mines.

Wilkins, R. A., and Bunn, E. S., 1943, Copper and copper base alloys: McGraw-Hill, New York, p. 7, chart 11.